SUPPORTING INFORMATION

Polyhydroxyanthraquinones as Quorum Sensing Inhibitors from the Guttates of *Penicillium restrictum* and Their Analysis by Desorption Electrospray Ionization Mass Spectrometry

Mario Figueroa, Alan K. Jarmusch, Huzefa A. Raja, Tamam El-Elimat, Jeffrey S. Kavanaugh, Alexander R. Horswill, R. Graham Cooks, Nadja B. Cech, and Nicholas H. Oberlies

CONTENTS

fragmentation of *m/z* 458 corresponding to the reactive DESI product annotated mass losses and proposed fragment ion structures.

Figure S8. A dose response curve of ω-hydroxyemodin (**3**) against quorum sensing reporter strain AH2759. Growth was assessed by absorbance readings at 600 nm after 15 h incubation (OD_{600}, blue), and bioluminescence was taken at that time point and plotted relative to growth (red). These data indicated that **3** did not significantly inhibit *S. aureus* growth in the concentration range tested as a quorum sensing inhibitor.

Transverse Sectioning of *P. restrictum* Culture Colony and Sample Preparation for DESI-MS Analysis.

Figure S9. Terms of location used in describing the *P. restrictum* DESI-MS imaging experiments. Transverse plane is defined here as being perpendicular to the anterior-posterior axis.

Figure S10. Schematic of imprinting experiment (from left to right): optical image of *P. restrictum* culture, PTFE imprint (pre-mass spectral analysis), representative DESI mass spectrum, and a plotted ion image corresponding to compound **2**, *m/z* 329.1.

Figure S11. Ion images corresponding to the pseudomolecular ($[M–H]^-$) ions of polyhydroxyanthraquinones **1–9** and optical image of PTFE imprint prior to imaging (upper left). Relative intensities ranging from blue (least abundant) to red (most abundant). The spatial distribution of **1–9** in the ion images and the imprint optical image regions were similar within the limits of the imprinting process. The topography of the culture caused certain regions of the fungal colonies to imprint poorly; for example, the middle region of the upper colony. Note, lines and imaging artifacts are present along the left side of the ion image due to variation in the surface-to-inlet distance. The image corresponding to compound **7** was complicated by an isobaric species that was present in the background.

Figure S12. DESI-MS ion images displaying additional ions whose spatial distribution correlate with *P. restrictum*. These ions are presumed to be of fungal origin, given that they were not observed in the analysis of guttate extracts and appear to correlate with fungal presence in the ion images.

Figure S13. (A) Optical image of a *P. restrictum* section post MS imaging, stained with hematoxylin and eosin. Fungal morphology, stained purple-blue, was detected and location of polyhydroxyanthraquinones was verified by unique alteration in dye color due to reduction-oxidation reactions, stained purple-red. (B) Overlay of two ions present in the mass spectrum, compound **3** (*m/z* 285.1) and **2** (*m/z* 329.1); the coloration of compound **3** ion image reflects relative abundance, whereas *m/z* 329.1 is displayed in grayscale to provide contrast. (C) Zoomed optical image of the region, indicated by red arrow, corresponding to polyhydroxyanthraquinone signal in B.

Figure S14. (A) ECD spectrum of compound **2** in a DMSO solution of $Mo_2(OAc)_4$ with inherent ECD spectra subtracted. (B) Conformation of the Mo_2^{4+} complex of **2**.

Figure S15. $\Delta\delta_H$ values [$\Delta\delta$ (in ppm) = $\delta_S - \delta_R$] obtained for (*S*)- and (*R*)-MTPA esters (**6a** and **6b**, respectively) of (+)-2'*S*-isorhodoptilometrin (**6**) in pyridine-d_5.

Figure S16. ^{1}H and ^{13}C NMR spectra of compound **1** [500 MHz for ^{1}H and 125 MHz for ^{13}C, methanol-d_4].

Figure S17. ^{1}H and ^{13}C NMR spectra of compound **2** [500 MHz for ^{1}H and 125 MHz for ^{13}C, methanol-d_4].

Figure S18. ^{1}H and ^{13}C NMR spectra of compound **3** [500 MHz for ^{1}H and 125 MHz for ^{13}C, DMSO-d_6].

Figure S19. ^{1}H and ^{13}C NMR spectra of compound **4** [500 MHz for ^{1}H and 125 MHz for ^{13}C, methanol-d_4].

Figure S20. ^{1}H and ^{13}C NMR spectra of compound **5** [500 MHz for ^{1}H and 125 MHz for ^{13}C, DMSO-d_6].

Figure S21. ^{1}H and ^{13}C NMR spectra of compound **6** [500 MHz for ^{1}H and 125 MHz for ^{13}C, methanol-d_4].

Figure S22. ^{1}H and ^{13}C NMR spectra of compound **7** [500 MHz for ^{1}H and 125 MHz for ^{13}C, DMSO-d_6].

Figure S23. ^{1}H and ^{13}C NMR spectra of compound **8** [500 MHz for ^{1}H and 125 MHz for ^{13}C, methanol-d_4].

Figure S24. ^{1}H$\rightarrow$^{13}C edited-HSQC NMR spectrum of compound **8** [500 MHz, methanol-d_4].

Figure S25. ^{1}H$\rightarrow$^{13}C HMBC NMR spectrum of compound **8** [500 MHz, methanol-d_4].

Figure S26. ^{1}H NMR spectrum of compound **9** [500 MHz , DMSO-d_6].

Macromorphological and Micromorphological Identification of the Fungal Strain.

Macromorphology. Colonies on YESD attained a diameter of 30–35 mm after 14 days at 25 °C, whereupon the colony appeared white, velvety, and showed sulcation with scalloped margins (Figure S1). The same colony after 16–21 days showed clear, white exudate droplets; colony reverse was yellowish in color. Colonies on MEA attained a diameter of 20–22 mm after 14 days at 25 °C. After 14 days the colony grown on MEA was white, velvety on the margins, and slight pinkish color inner margins. The colony formed bright red color exudate droplets with reverse light reddish-brown. The red-brown pigment often diffused in the agar medium after 21 days. Colonies on PDA attained a diameter of 20–25 mm after 14 days at 25 °C. It was white with velvety margins and formed bright red color exudate droplets; colony reverse was light reddish-brown due to soluble pigment diffusing in the agar medium after 21 days. The soluble pigment was often seen only on MEA and PDA media.

Micromorphology. Conidiophores hyaline, short, smooth-walled arise from aerial hyphae, strictly monoverticillate, and nonvesiculate, 13–25 × 2–3 μm; with an apical whorl of 3–5, ampulliform phialides, 3–6 × 2–4 μm. Conidia born in chains, hyaline to greenish, globose to subglobose, smooth walled based on light microscopy, 2–3 μm. Based on the morphological identification, we assigned the fungus G85 to *Penicillium restrictum* (Trichocomaceae, Eurotiales, Eurotiomycetideae, Eurotiomycetes, Ascomycota).

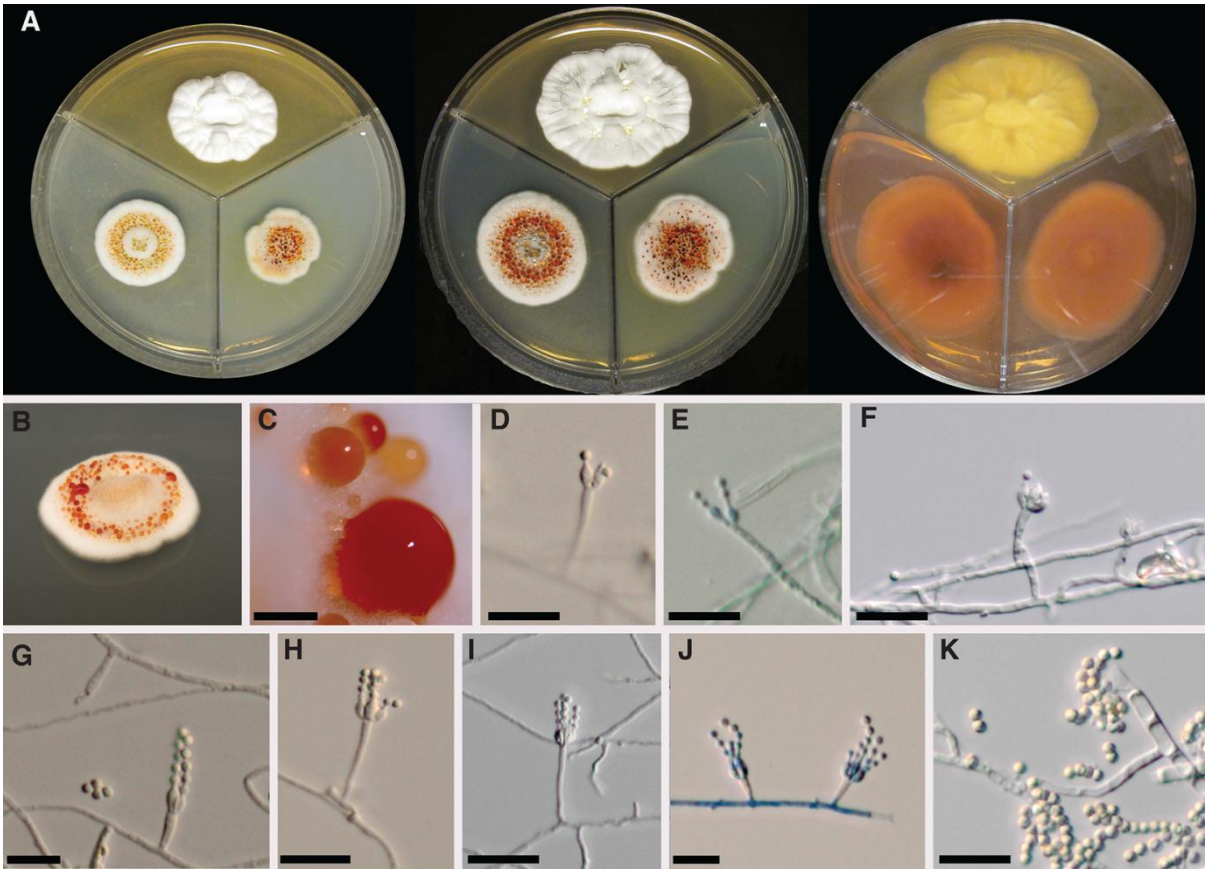

Figure S1. *Penicillium restrictum*. (A) Colonies of G85 grown on different nutrient media; 10 day old culture; 16 day old culture; 21 day old culture in reverse. Clock-wise top panel YESD, right panel MEA, and left panel PDA. For reverse colonies, clock-wise top panel YESD, right panel PDA, and left panel MEA. (B) A 14 day old culture on PDA with antibiotics. (C) Close up of exudate droplets on PDA. (D–K) Conidiophore and conidia of *P. restrictum*.

Molecular Identification and Phylogenetic Analysis of the Fungal Strain.

Molecular Identification. For identification of the fungal strain G85, the complete internal transcribed spacer regions 1 & 2 and 5.8S nrDNA (ITS) along with the D1/D2 variable domains (partial region of large subunit of the 28S nuclear ribosomal DNA, LSU) were sequenced, as detailed previously.[2] For extraction of genomic DNA, mycelium from axenic cultures grown in YESD broth was scraped with a sterile scalpel and ground to a fine powder in liquid nitrogen using a mortar and pestle. Approximately 400 μL of AP1 buffer from the DNAeasy Plant Mini Kit (QIAGEN, Inc.) were added to the mycelial powder, and DNA was extracted following the manufacturer's instructions. The DNA was finally eluted in approximately 25–30 μL distilled water. The complete ITS region along with D1/D2 variable domains were amplified with ITS1F and LR3 by PCR using puReTaq™ Ready-To-Go PCR beads (Amersham Biosciences Corp.) and subsequently sequenced in 11 μL sequencing reactions with BigDye® Terminators v3.1 (Applied Biosystems) using ITS primers ITS1F and ITS4[3,4] and LSU primers LROR and LR3.[5,6] For PCR, the following protocol was utilized: initial denaturation at 95 °C for 5 min, followed by 35 or 40 cycles of 95 °C for 30 s, 41 or 50 °C for 15 s, and 72 °C for 1 min with a final extension step of 72 °C for 10 min. To enhance the PCR reactions, 2.5 μL of BSA (bovine serum albumin, New England Biolabs) and/or 2.5 μL of DMSO (dimethyl sulfoxide, Fisher Scientific) were added. The PCR products were purified to remove excess primers, dNTPs, and nonspecific amplification products with the QIAquick PCR Purification Kit (QIAGEN Inc.). Sequences were generated on an Applied Biosystems 3730XL high-throughput capillary sequencer at the University of Illinois Urbana-Champaign Biotech facility. The sequences were downloaded from GenBank that had the closest similarity with ITS-LSU sequence of G85, and Maximum Likelihood (ML) phylogenetic analysis was employed to determine the phylogenetic affinities

with other *Penicillium* spp. Multiple sequence alignment and phylogenetic analysis was performed following programs reviewed by Schmitt and Barker.[7]

Phylogenetic Analysis. Based on a megablast search of NCBIs GenBank nucleotide database, the closest hit using the ITS-LSU sequence was *Penicillium restrictum* (GenBank AF033459; Identities = 1117/1122 (99 %), Gaps = 1/1122 (0 %)), followed by *P. restrictum* (GenBank AF033457; Identities = 1116/1122 (99 %), Gaps = 1/1116 (0 %)), and *P. kurssanovii* (GenBank EF422849; Identities = 1111/1116 (99 %), Gaps = 0/1116 (0 %). Other members, which also had identities with 99% similarity included, *Eupenicillium katangense* (GenBank AF033458); *Eupenicillium meridianum* (GenBank AF03345); *P. citreonigrum* (GenBank AF033456); *E. alutaceum* (GenBank AF033454); *P. terrenum* (GenBank AF033446); *P. velutinum* (GenBank AF033448); *P. namyslowskii* (GenBank AF033463); *P. citreonigrum* (GenBank EF198647); *Penicillium* sp. (GenBank AF125942); *P. melinii* (GenBank AF033449); *P. toxicarum* (GenBank EF198645), and *P. carylophilum* (GenBank AF034457). Maximum Likelihood analysis indicated that G85 shared phylogenetic affinities with clade 10 of section *Exilicaulis* Pitt [1] and group 4 sensu,[8] which consists of predominantly monoverticillate species (Figure S2).

In addition to the ITS region, the ribosomal polymerase II subunit 2 (RPB2) gene was used to obtain a species level identification of G85. It was recently suggested by Peterson[9] that ITS barcodes may be problematic and not yield an accurate species level identification for certain members of the family Trichocomaceae. The RPB2 gene has been used successfully for inferring species-level phylogenetic relationships and identifications of *Penicillium* sp.[1] Sequence data for the RPB2 region are available in NCBI GenBank for a number type strains of *Penicillium* spp. Thus, the RPB2 gene was sequenced using primers and PCR protocols using methods outlined previously.[10] Sequences were generated on an Applied Biosystems 3730XL

high-throughput capillary sequencer at the University of Illinois Urbana-Champaign Biotech facility. For the phylogenetic analysis, RPB2 sequences of *Penicillium* spp. clade 10 of section *Exilicaulis* Pitt[1] and group 4 sensu Pitt,[9] which consists of predominantly monoverticillate species, were downloaded from GenBank. Multiple sequence alignment and Maximum Likelihood analysis with RPB2 sequences were run using programs reviewed by Schmitt and Barker.[7] Robustness of clades was analyzed using 1000 bootstrap replicates using evolutionary phylogenetic analysis software MEGA.[11] Clades with bootstrap support ≥70% was considered significant and strongly supported.[12] Based on the results of phylogenetic analysis of RPB2 sequences from strain G85 with type strains of monoverticillate species, it was concluded that G85 belonged to *Penicillium restrictum*. Sequences of strain G85 form a strongly supported (96% ML bootstrap support) monophyletic clade with the neotype strain of *P. restrictum* (CBS 367.48)[1] (Figure S3).

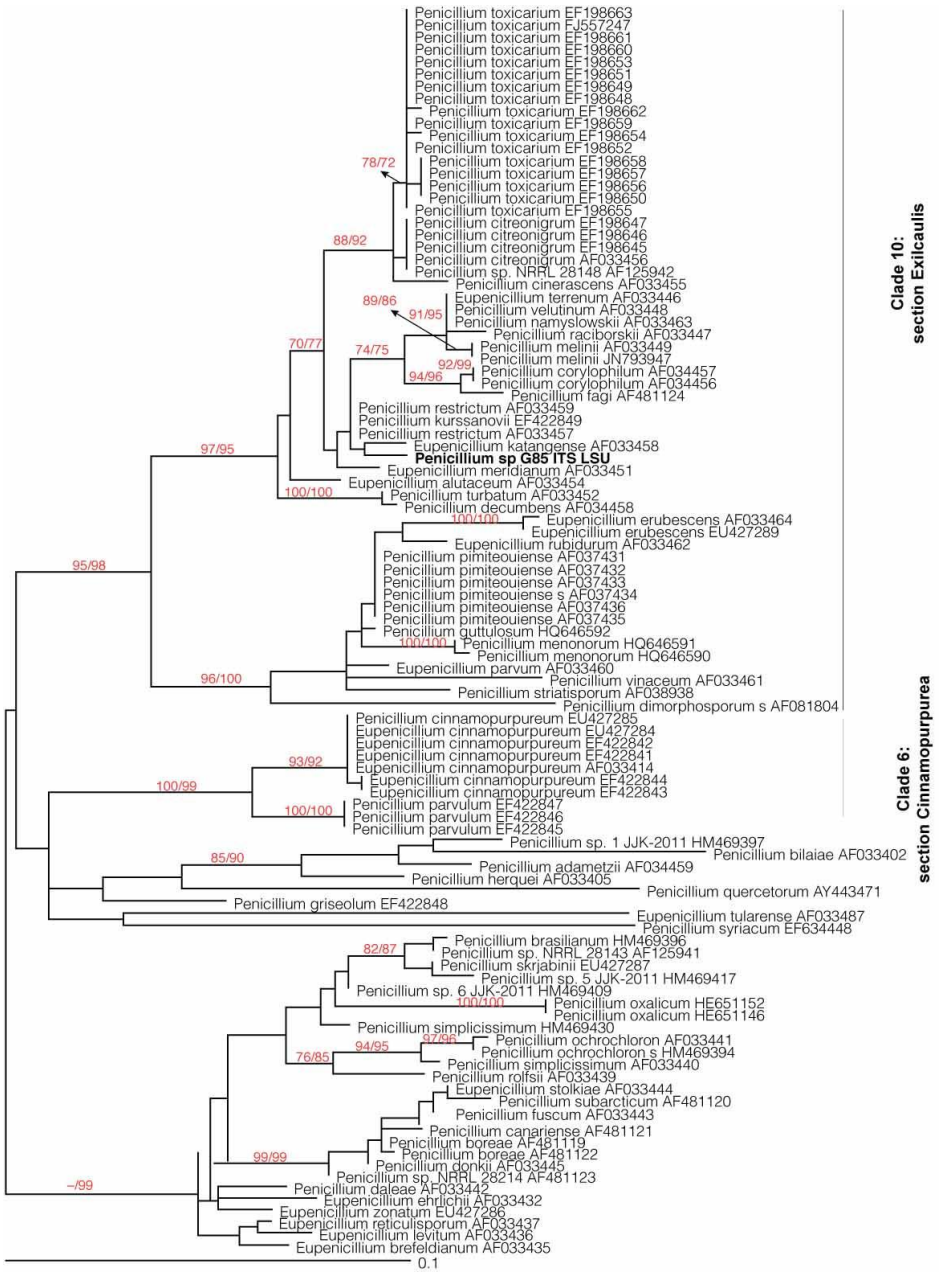

Figure S2. Phylogram of the most likely tree (–lnL = 4318.90) from a PHYML analysis of 101 taxa based on combined ITS and LSU nrDNA (1121 bp). Numbers on the branches refer to PHYML/RAxML bootstrap support values ≥ 70% based on 1000 replicates. Classification following Houbraken and Samson[1] is shown on the right. Bar indicates nucleotide substitutions per site.

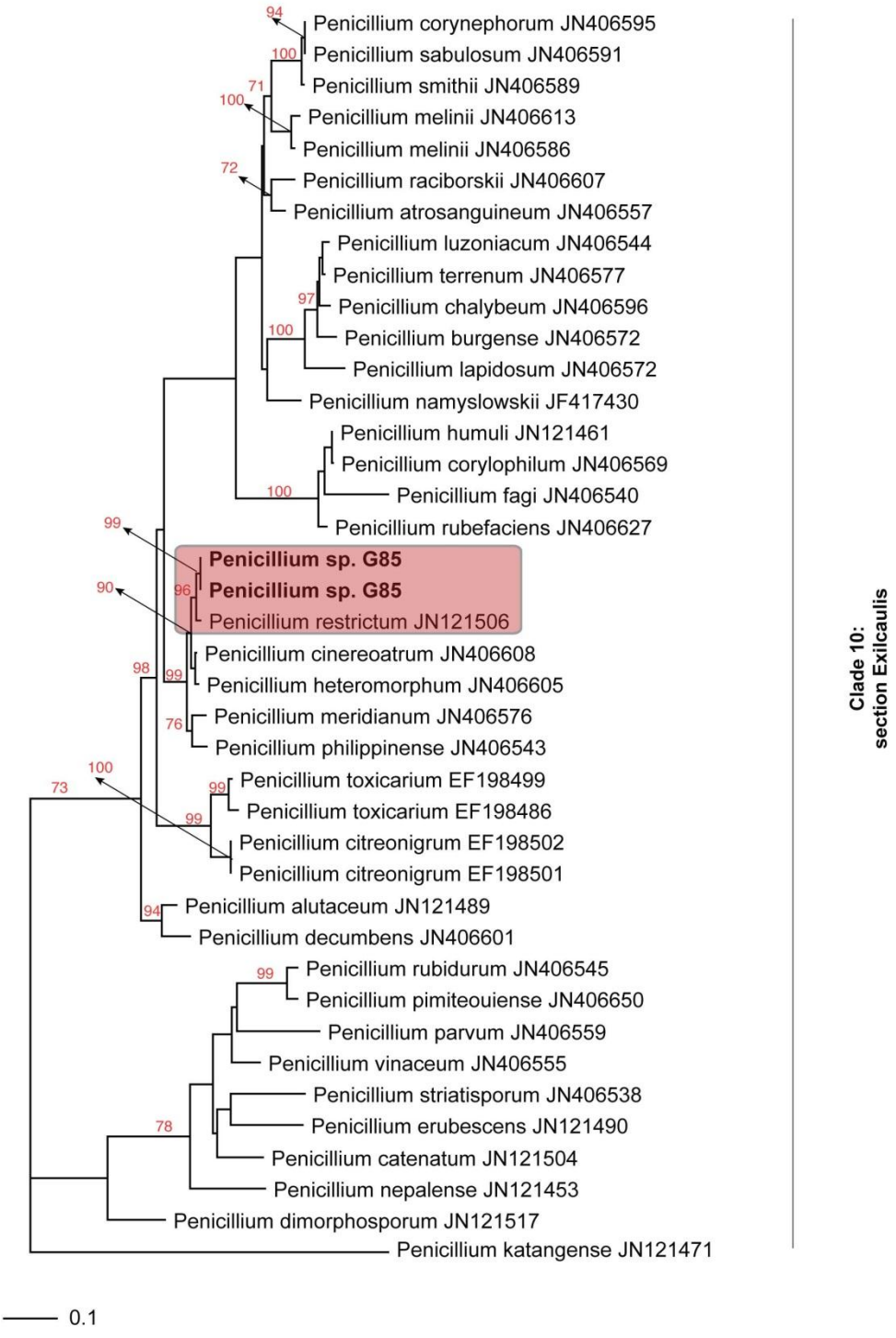

Figure S3. Phylogram of the most likely tree (–lnL = 6337.14) from a PHYML analysis of 40 taxa based on combined RPB2 sequence data (914 bp). Numbers on the branches refer to ML bootstrap support values ≥ 70% based on 1000 replicates. Classification following Houbraken and Samson[1] is shown on the right. Bar indicates nucleotide substitutions per site.

Solid Phase Culture Methods. A piece of a fresh culture grown in MEA medium was transferred to a liquid medium containing 2% soy peptone, 2% dextrose and 1% yeast extract (YESD medium). Following incubation (7 days) at 22 °C with agitation, the culture was used to inoculate ~10 g of rice medium, to which was added ~30 mL of H_2O, in a 250 mL Erlenmeyer flask. This was replicated in a total of four Erlenmeyer flasks, and all were incubated at 22 °C until the cultures showed good growth (14 d).[13]

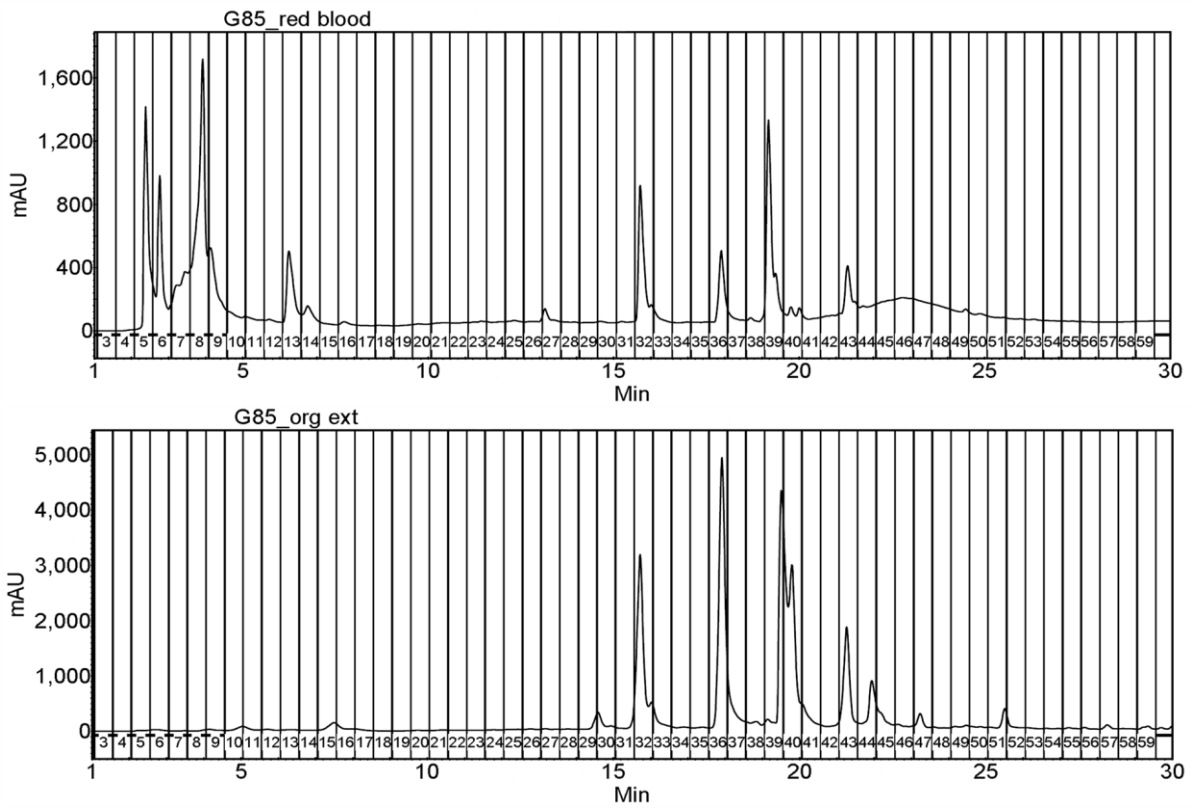

Figure S4. Typical semiprep-HPLC chromatograms (UV 254 nm) of guttates of *P. restrictum* (upper panel) versus MeOH–CH_3CN fraction from the solid phase culture (lower panel). Both samples (3 and 10 mg of guttate and MeOH–CH_3CN fraction, respectively) were analyzed using a Gemini-NX (5 μm, 250 × 10 mm; Phenomenex) column via a linear gradient from 20 to 100% CH_3CN in 0.1% aqueous formic acid over 30 min at a flow rate of 3.5 mL/min.

Methods and Characterization of Compounds.

Isolation of Compounds 1–9. The MeOH–CH_3CN fraction (300 mg out of ~1 g of total material) was dissolved in a mixture MeOH–Dioxane (1:1) and then subjected to preparative HPLC (Gemini NX column, 20–100% CH_3CN in 0.1% aqueous formic acid over 30 min; fractions collected every 0.5 min). Compounds **1–9** were collected as follow (see Figure 1): **1** (fr. 11-12, 2.7 mg), **2** (fr. 15-16, 27.7 mg), **3** (fr. 25-27, 19.1 mg), **4** (fr. 30, 5.5 mg), **5** (fr. 32-33, 8.4 mg), **6** (fr. 35, 4.6 mg), **7** (fr. 40, 6.1 mg), **8** (fr. 41, 4.0 mg), **9** (fr. 54, 1.0 mg).

Structure Determination of the Polyhydroxyanthraquinones 1–9. The identification of known compounds ω-hydroxyemodin (**3**), emodic acid (**5**), and emodin (**9**), was based on comparisons of NMR and HRMS data with those reported previously (see Results and Discussion section for references and NMR spectra). The structures of the new compounds (**1**, **2**, **4**, **7**, and **8**) were elucidated as delineated below. The characterization of (+)-2'*S*-isorhodoptilometrin (**6**) was also described in detail below, since this was the first report of its absolute configuration.

Compound (**1**) was obtained as a red amorphous solid after final C_{18} HPLC purification, and its molecular formula was established as $C_{15}H_8O_8$ by ESI-HRMS measurements (obsd $[M–H]^-$ *m/z* 315.0147, calcd for $C_{15}H_7O_8$, 315.0146) (Figure S5). The ^{1}H NMR spectrum of **1** (Table S1, Figure S16) showed characteristic resonances for three aromatic protons at δ_H 7.29, 7.73 and 8.23, for H-4, H-7, and H-5, respectively. Compound **1** was clearly related to the other known polyhydroxyanthraquinones (**3**, **5**, **6**, and **9**), especially to compound **5**. The lack of an aromatic H-2 signal at δ_H 6.54, as observed in **5**, and the HMBC correlations (Figure S6) from H-4 to C-2 (δ_C 138.9), C-9a (δ_C 110.3) and C-10 (δ_C 180.6); from H-7 to C-8a (δ_C 117.4), C-5 (δ_C 119.4) and C-1' (δ_C 168.6); and from H-5 to C-8a, C-7 (δ_C 123.8), C-1', and C-10, were critical in

determining the complete structure of **1** as a 6-substituded-1,2,3,8-tetrahydroxy anthraquinone. Ultimately, the new compound **1** was elucidated as 1,2,3,8-tetrahydroxy-9,10-dioxo-9,10-dihydroanthracene-6-carboxylic acid, and given the trivial name of 2-hydroxyemodic acid.

Compound **2** was isolated as a red amorphous powder. Its molecular formula, $C_{17}H_{14}O_7$, was deducted by HRESIMS ($[M-H]^-$ obs *m/z* 329.0662, calcd for $C_{17}H_{13}O_7$, 329.0667) (Figure S5). The ^1H and ^{13}C NMR spectra of **2** (Table S1, Figure S17) showed resonances similar to those of compound **6**, but changes in the aliphatic side were obvious. For example, the methylene at C-1' (δ_C 45.2 and δ_H 2.78, d, J = 6.3 Hz) observed in **6** was replaced with an oxymethine (δ_C 77.0 and δ_H 4.51, d, J = 5.2) in **2**, and the oxymethine at C-2' (δ_C 67.6 and δ_H 4.02, m) in **6** was shifted downfield to δ_C 70.8 (δ_H 3.86, qd, J = 5.7, 6.8 Hz) in **2**. In the HMBC spectrum (Figure S6), key correlations were observed from H-5 (δ_H 7.66, s) to C-1', C-8a (δ_C 114.5), C-7 (δ_C 122.1), and C-10 (δ_C 181.5); from H-7 (δ_H 7.22, s) to C-1', C-8a, C-5 (δ_C 118.7), and C-8 (δ_C 161.8); from H-4 (δ_H 7.01, d, J = 2.3) to C-10 and C-9a (δ_C 109.0); and from H-2 (δ_H 6.40, d, J = 2.3) to C-4 (δ_C 108.8), and C-3 (δ_C 165.8) (Table S1). The oxymethines of the side chain showed HMBC correlations from H-1' to C-3' (δ_C 17.1), C-2' (δ_C 70.8), C-5, C-7, and C-6 (δ_C 152.2); and from H-2' with C-6, respectively, and the terminal methyl group CH_3-3' showed correlations with C-2' and C-1'. Finally, COSY correlations were observed between H-1' and H-2', and H-2' and CH_3-3'. The absolute configuration of **2** having a *sec*/*sec*-1,2-diol moiety was examined using the *in situ* dimolybdenum CD method developed by Snatzke and Frelek.[14-16] After the addition of dimolybdenum tetraacetate [$Mo_2(AcO)_4$] in DMSO to compound **2**, a metal complex was generated as an auxiliary chromophore. The observed sign of the Cotton effects in the induced circular dichroism (ICD) spectrum originates solely from the chirality of the *sec*/*sec*-1,2-diol

moiety expressed by the sign of the O–C–C–O torsion angle in the favored conformation (Figure S14B). The positive and negative Cotton effects observed at around 310 (band IV) and 400 nm (band II), respectively (Figure S14A), suggested assignment of the 1'*S* and 2'*R* configuration on the basis of the empirical rule proposed by Snatzke. The *cis*-diol coplanar geometry of the 1,2-dihydroxypropyl side chain of **2** was also confirmed by reactive DESI analysis[17] using dimethylaminophenylboronic acid (Figure S7).[18] The predicted reaction product, polyhydroxyquinone-arylboronate ester, was observed by characteristic MS^2 fragmentation, as well as the loss of the aryl boronate (Figure S7). On the basis of these data, compound **2** was elucidated as 6-(1*S*,2*R*-dihydroxypropyl)-1,6,8-trihydroxyanthracene-9,10-dione, and given the trivial name of 1'-hydroxyisorhodoptilometrin.

Compound **4** was isolated as a red amorphous solid. The HRESIMS spectrum suggested a formula of $C_{17}H_{12}O_7$ (obsd $[M-H]^-$ *m/z* 327.0511, calcd for $C_{17}H_{11}O_7$, 327.0510) (Figure S5). The UV and ^1H NMR spectra suggested that **4** belonged to the same family of natural products. The primary differences in the ^1H NMR (Table S1, Figure S19) spectra of **4** were the lack of the oxymetine resonance observed at δ_H 3.96 (H-2') in **2**, and the downfield shifted oxymethine H-1' (δ_H 5.20, s) and CH_3-3' (δ_H 2.15, s) resonances, the latter were both associated to the presence of an additional carbonyl moiety at C-2' (δ_C 207.4). The HMBC correlations (Figure S6) from H-5 (δ_H 7.75, s), H-7 (δ_H 7.32, s), and H-3' to C-1' (δ_C 79.0); from H-1' to C-5 (δ_C 117.3), C-7 (δ_C 121.7), C-6 (δ_C 148.1), and C-2' (δ_C 207.4); and from H-3' to C-2', confirmed the structure of the side chain in **4**. In addition, the correlations from H-2 (δ_H 6.50, s) to C-4 (δ_C 109.0), C-1 (δ_C 165.3), and C-3 (δ_C 166.3); from H-4 (δ_H 7.12, s) to C-9a (δ_C 108.9) and C-10 (δ_C 181.3); from H-7 to C-5; and from H-5 to C-8a (δ_C 115.2), C-7, and C-10 were consistent with the location of

the side chain as well as the 6-substituded-1,3,8-trihydroxy anthraquinone core. Accordingly, compound **4** was established as 1,3,8-trihydroxy-6-(1-hydroxy-2-oxopropyl)anthracene-9,10-dione and given the trivial name of 1'-hydroxy-2'-ketoisorhodoptilometrin. An attempt to establish the absolute configuration via a modified Mosher's ester method[19] was unsuccessful due to degradation of the compound.

(+)-2'*S*-Isorhodoptilometrin (**6**) was isolated as an orange powder with a molecular formula of $C_{17}H_{14}O_6$ as determined by HRESIMS and analysis of ^{1}H NMR, ^{13}C NMR, and edited-HSQC data (Table S1, Figures S5 and S21). The NMR data of compound **6** were found to be in agreement with that reported of isorhodoptilometrin, a polyhydroxyanthraquinone that was isolated from a marine-crinoid *Ptilometra australis*,[20] a marine-derived fungus *Trichoderma aureoviride*,[21] and a marine lichen-derived fungus *Gliocladium* sp.[22] Compound **6**, opposite to isorhodoptilometrin isolated by Khamthong and collaborators,[21] was found to be dextrorotatory. As such, the absolute configuration of **6** was assigned as 2'*S* via the modified Mosher's ester method (Figure S15);[19] this represented the first report of the characterization of the absolute configuration of **6**.

Compound **7** was isolated as a red amorphous solid, and its molecular formula was found to be $C_{17}H_{12}O_6$ on the basis of HRESIMS (obsd $[M-H]^-$ *m/z* 311.0560, calcd for $C_{17}H_{11}O_6$, 311.0561; Figure S5), indicating 12 degrees of unsaturation, which was one greater than that of **6**. The ^{1}H and ^{13}C NMR spectroscopic data of **7** (Table S1, Figure S22) were also slightly different from those of **6**. An oxymethine moiety (δ_H/δ_C 4.02/67.6) in **6** was replaced by a ketone (δ_C 205.3), indicating oxidation of the secondary alcohol in **7** relative to **6**. A methyl doublet (δ_H/δ_C

1.21/22.0) in **6** was replaced by a downfield shifted singlet methyl (δ_H/δ_C 2.18/30.5) in **7**, and a methylene doublet (δ_H/δ_C 2.78/45.2) in **6** was replaced by a downfield shifted methylene singlet (δ_H/δ_C 4.0/49.6) in **7**. Key HMBC correlations for **7** are highlighted in Figure S6. Consequently, compound **7** was determined to be 1,3,8-trihydroxy-6-(2-oxopropyl)anthracene-9,10-dione1,3,8-trihydroxy-6-(2-oxopropyl)anthracene-9,10-dione and given the trivial name of desmethyl dermoquinone.

Compound **8** was isolated as a red amorphous solid. The molecular formula of $C_{15}H_7ClO_7$ was established by HRESIMS, where a $[M-H]^-$ ion peak at *m/z* 332.9803 and an $[M-H+2]^-$ isotopic peak at *m/z* 334.9774 (calcd for $C_{15}H_6{}^{35}ClO_7$, 332.9808 and for $C_{15}H_6{}^{37}ClO_7$, 334.9778, respectively; Figure S5) supported the presence of a chlorine atom. A key difference in the NMR data of compound **8**, relative to that of **5**, was the absence of a signal for H-2 in the spectrum of **8**. Moreover, the downfield shifted ^{13}C resonance of C-2 relative to the same position in **5** further supported the presence of C-2 chloro substitution in **8** (Table S1, Figures S20 and S23-S25). Therefore, **8** was established as 2-chloro-1,3,8-trihydroxy-9,10-dioxo-9,10-dihydroanthracene-2-carboxylic acid and given the trivial name of 2-chloroemodic acid. Arioka et al.[23] reported the inhibitory activity of **8** against *Trypanosoma cruzi* trans-sialidase (TcTS), however, the source and spectroscopic data for this compound were not described. Finally, Kemami Wangun and collaborators reported the 2-bromo-derivative of **5** from a deep-water crinoid, *Holopus rangii*.[24]

2-Hydroxyemodic acid (**1**): red amorphous solid; UV (MeOH) λ_{max} (log ε) 433 (3.54), 289 (3.79), 222 (3.79) nm; IR (diamond) ν_{max} 2920, 1703, 1621, 1548, 1459, 1354, 1255, 1082, 1032,

977, 819, 747 cm^{-1}; ^{1}H and ^{13}C NMR (in methanol-d_4 at 500 and 125 MHz, respectively), see Table S1 and Figure S16; HRESIMS *m/z* 315.0147 $[M–H]^-$ (calcd for $C_{15}H_7O_8$, 315.0146; Figure S5).

1'-Hydroxyisorhodoptilometrin (**2**): red amorphous solid; $[\alpha]_D^{24}$ –35 (*c* 0.2, MeOH); UV (MeOH) λ_{max} (log ε) 437 (3.95), 290 (4.47), 253 (4.13), 223 (4.18) nm; CD (*c* 7.57 × 10^{-5} M, MeOH) λ_{max} ($\Delta\varepsilon$) 217 (–4.56), 233 (+5.40), 249 (–2.70), 274 (+3.33), 289 (–1.11), and 300 (+1.53) nm; IR (diamond) ν_{max} 2973, 1672, 1621, 1561, 1474, 1392, 1364, 1254, 1212, 987, 759 cm^{-1}; ^{1}H and ^{13}C NMR (in methanol-d_4 at 500 and 125 MHz, respectively), see Table S1 and Figure S17; HRESIMS *m/z* 329.0662 $[M–H]^-$ (calcd for $C_{17}H_{13}O_7$, 329.0667; Figure S5).

1'-Hydroxy-2'-ketoisorhodoptilometrin (**4**): red amorphous solid; $[\alpha]_D^{24}$ +6 (*c* 0.07, MeOH); UV (MeOH) λ_{max} (log ε) 435 (3.69), 250 (3.84), 225 (3.90) nm; CD (*c* 7.62 × 10^{-5} M, MeOH) λ_{max} ($\Delta\varepsilon$) 212 (–6.19), 229 (+6.98), 242 (–3.08), 246 (+2.28), 261 (–3.23), 280 (+2.07), 291 (–0.29), and 300 (+1.25) nm; IR (diamond) ν_{max} 3368, 2949, 2838, 1627, 1464, 1382, 1269, 1213, 1113, 1014, 754 cm^{-1}; ^{1}H and ^{13}C NMR (in methanol-d_4 at 500 and 125 MHz, respectively), see Table S1 and Figure S19; HRESIMS *m/z* 327.0509 $[M–H]^-$ (calcd for $C_{17}H_{11}O_7$, 327.0510; Figure S5).

(+)-2'*S*-Isorhodoptilometrin (**6**): orange amorphous solid; $[\alpha]_D^{24}$ +30 (*c* 0.13, MeOH); UV (MeOH) λ_{max} (log ε) 440 (3.72), 290 (3.85), 253 (3.85), 225 (3.84) nm; IR (diamond) ν_{max} 3382, 2965, 1673, 1608, 1564, 1465, 1397, 1359, 1270, 1221, 1168, 1049, 857, 755 cm^{-1}; ^{1}H and ^{13}C NMR (in methanol-d_4 at 500 and 125 MHz, respectively), see Table S1 and Figure S21; HRESIMS *m/z* 313.0715 $[M–H]^-$ (calcd for $C_{17}H_{13}O_6$, 313.0718; Figure S5).

Desmethyl dermoquinone (**7**): red amorphous solid; UV (MeOH) λ_{max} (log ε) 436 (3.76), 288 (3.96), 251 (3.98), 223 (4.10) nm; ^{1}H and ^{13}C NMR (in DMSO-d_6 at 500 and 125 MHz, respectively), see Table S1 and Figure S22; HRESIMS *m/z* 311.0560 $[M–H]^-$ (calcd for $C_{17}H_{11}O_6$, 311.0561; Figure S5).

2-Chloroemodic acid (**8**): red amorphous solid; UV (MeOH) λ_{max} (log ε) 435 (3.46), 258 (3.78), 222 (3.88) nm; IR (diamond) ν_{max} 3076, 2344, 1678, 1619, 1554, 1473, 1384, 1246, 1213, 1019, 913, 751 cm^{-1}; ^{1}H and ^{13}C NMR (in methanol-d_4 at 500 and 125 MHz, respectively), see Table S1 and Figures S23-S25; HRESIMS *m/z* 332.9803 $[M–H]^-$ and *m/z* 334.9774 $[M−H+2]^-$ (calcd for $C_{15}H_6O_7{}^{35}Cl$, 332.9808 and *m/z* 334.9778 $[M−H+2]^-$, respectively; Figure S5).

Preparation of the (*R*)- and (*S*)-MTPA ester derivatives of (+)-2'*S*-isorhodoptilometrin (6): To 0.60 mg of compound **6** was added 400 μL of pyridine-d_5 and transferred into an NMR tube. To initiate the reaction, 10 μL of *S*-(+)-α-methoxy-α-(trifluoromethyl)phenylacetyl (MTPA) chloride was added into the NMR tube with careful shaking and then monitored immediately by ^{1}H NMR at the following time points: 0, 5, 10, and 15 min. The reaction was found to be complete within 5 min, yielding the mono (*R*)-MTPA ester derivative (**6b**) of **6**. ^{1}H NMR data of **6b** (500 MHz, pyridine-d_5): δ_H 1.42 (3H, d, J = 6.9, H_3-3′), 3.00 (2H, d, J = 6.9, H_2-1′), 5.61 (1H, sextet, J = 6.9, H-2′). In an analogues manner, 0.60 mg of compound **6** dissolved in 400 μL pyridine-d_5 was reacted in a second NMR tube with 10 μL (*R*)-(−)-a-MTPA chloride for 5 min, to afford the mono (*S*)-MTPA ester (**6a**). ^{1}H NMR data of **6a** (500 MHz, pyridine-d_5): δ_H 1.34 (3H, d, J = 6.9, H_3-3′), 3.06 (2H, d, J = 6.9, H_2-1′), 5.61 (1H, sextet, J = 6.9, H-2′).

Determination of the absolute configuration of an acyclic 1,2-diol moiety in 2 using Snatzke's method. The absolute configuration of the acyclic 1,2-diol moiety in **2** was determined using Snatzke's method.[16,25,26] Briefly, to a 2.5 mL of 0.32 mM stock solution of $[Mo_2(AcO)_4]$ in DMSO, was added 2.5 mL of **2** (0.03 mM). ECD spectra were collected immediately after mixing every 10 min for 1 h.

Table S1. NMR data for compounds 1, 2, 4, and 6–8 (^{1}H and ^{13}C were run at 500 and 125 MHz, respectively) in methanol-d_4 for compounds 1, 2, 4, 6, and 8, and in DMSO-d_6 for compound 7

	1		**2**		**4**	
position	δ_C, type	δ_H, mult (*J* in Hz)	δ_C, type	δ_H, mult (*J* in Hz)	δ_C, type	δ_H, mult (*J* in Hz)
1	151.5, C		165.1, C		165.3, C	
2	138.9, C		107.6, CH	6.40, d (2.3)	107.7, CH	6.50, d (2.2)
3	153.2, C		165.8, C		166.3, C	
4	109.3, CH	7.29, s	108.8, CH	7.01, d (2.3)	109.0, CH	7.12, d (2.2)
4a	125.6, C		135.3, C		135.3, C	
5	119.4, CH	8.23, s	118.7, CH	7.66, s	117.3, CH	7.75, s
6	138.3, C		152.2, C		148.1, C	
7	123.8, CH	7.73, s	122.1, CH	7.22, s	121.7, CH	7.32, s
8	161.8, C		161.8, C		162.1, C	
8a	117.4, C		114.5, C		115.2, C	
9	191.4, C		190.3, C		190.3, C	
9a	110.3. C		109.0, C		108.9, C	
10	180.6, C		181.5, C		181.3, C	
10a	133.8, C		132.9, C		133.6, C	
1'	168.6, C		77.0, CH	4.51, d (5.2)	79.0, CH	5.20, s
2'			70.8, CH	3.86, qd (5.7, 6.8)	207.4, C	
3'			17.1, CH_3	1.16, d (6.3)	24.1, CH_3	2.15, s

	6		**7**		**8**	
position	δ_C, type	δ_H, mult (*J* in Hz)	δ_C, type	δ_H, mult (*J* in Hz)	δ_C, type	δ_H, mult (*J* in Hz)
1	165.4, C		166.8, C		160.7, C	
2	107.8, CH	6.51, d (2.9)	108.5, CH	6.54, d (2.3)	113.8, C	
3	167.0, C		165.1, C		160.9, C	
4	109.3, CH	7.15, d (2.9)	109.7, CH	7.09, d (2.3)	109.9[a], CH	7.26, s
4a	135.5, C		135.6, C		132.6, C	
5	120.7, CH	7.61, d (1.2)	121.7, CH	7.49, d (1.7)	119.7, CH	8.26, s
6	149.3, C		145.3, C		141.5, C	
7	124.5, CH	7.13, d (1.2)	125.9, CH	7.14, d (1.7)	124.2, CH	7.75, s
8	162.0, C		161.7, C		162.0, C	
8a	114.0, C		114.8, C		117.3, C	
9	190.4, C		190.1, C		189.7, C	
9a	108.8, C		109.3, C		108.1[a], C	
10	182.0, C		182.1, C		181.4, C	
10a	133.3, C		133.3, C		133.4, C	
1'	45.2, CH_2	2.78, d (6.3)	49.6, CH_2	4.0, s	169.3[a], C	
2'	67.6, CH	4.02, sextet (6.3)	205.3, C			
3'	22.0, CH_3	1.21, d (6.3)	30.5, CH_3	2.18, s		

[a] Confirmed by HMBC.

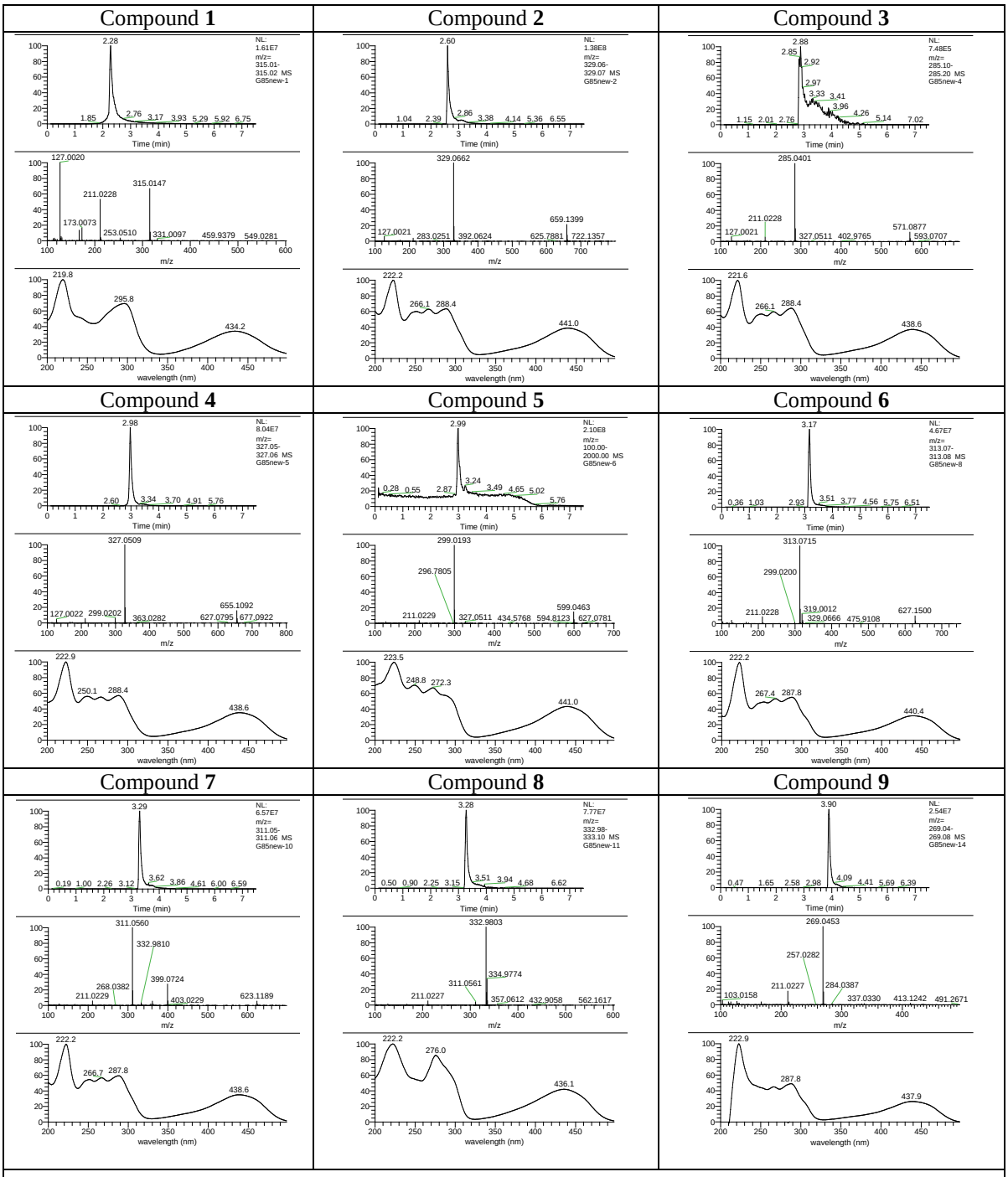

Figure S5. UPLC-(–)-ESI-HRMS data for pure compounds **1–9**. For each compound, the upper panel shows the TIC chromatogram at a specific mass range; the middle panel shows the high resolution mass spectrum; and the bottom panel shows the UV-PDA spectrum (200–500 nm).

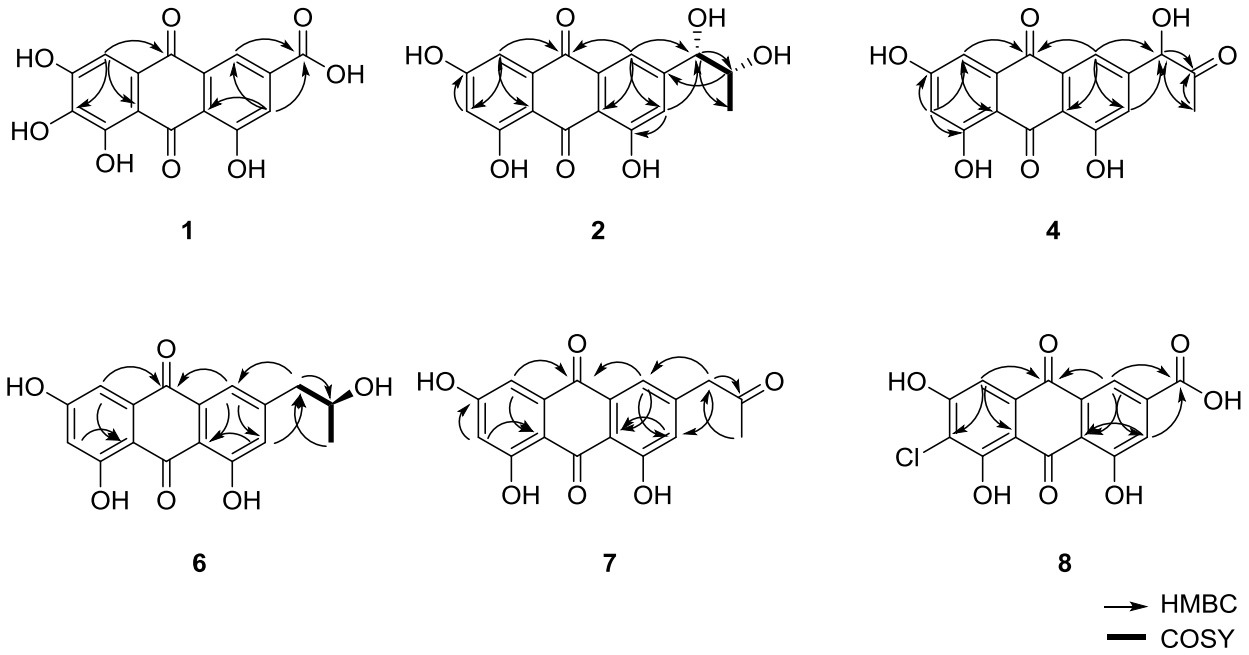

Figure S6. Key HMBC and COSY correlations for compounds **1**, **2**, **4**, and **6–8**.

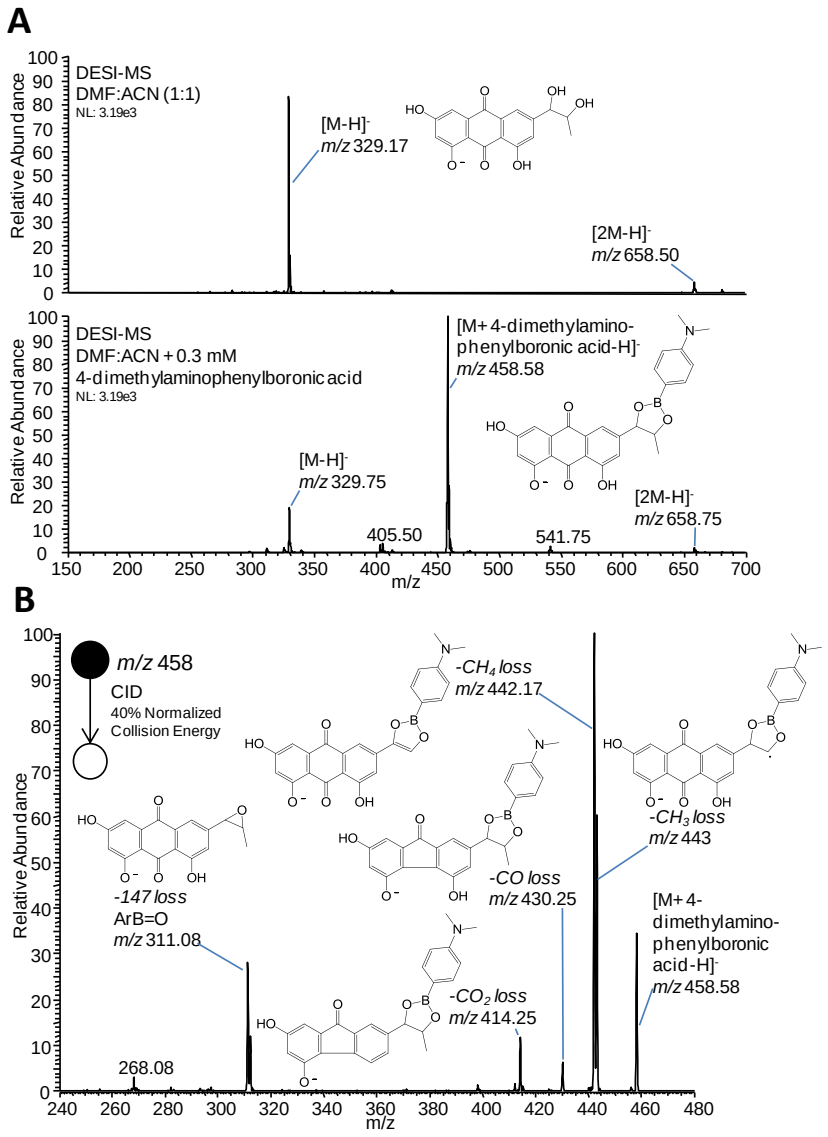

Figure S7. (A) Upper: Mass spectrum of compound **2** acquired by DESI using non-reactive solvents [DMF–CH_3CN (1:1)]; Lower: Mass spectrum of compound **2** analyzed by reactive DESI using DMF–CH_3CN containing 0.3 mM 4-dimethylaminophenylboronic acid; (B) MS^2 fragmentation of *m/z* 458 corresponding to the reactive DESI product annotated mass losses and proposed fragment ion structures.

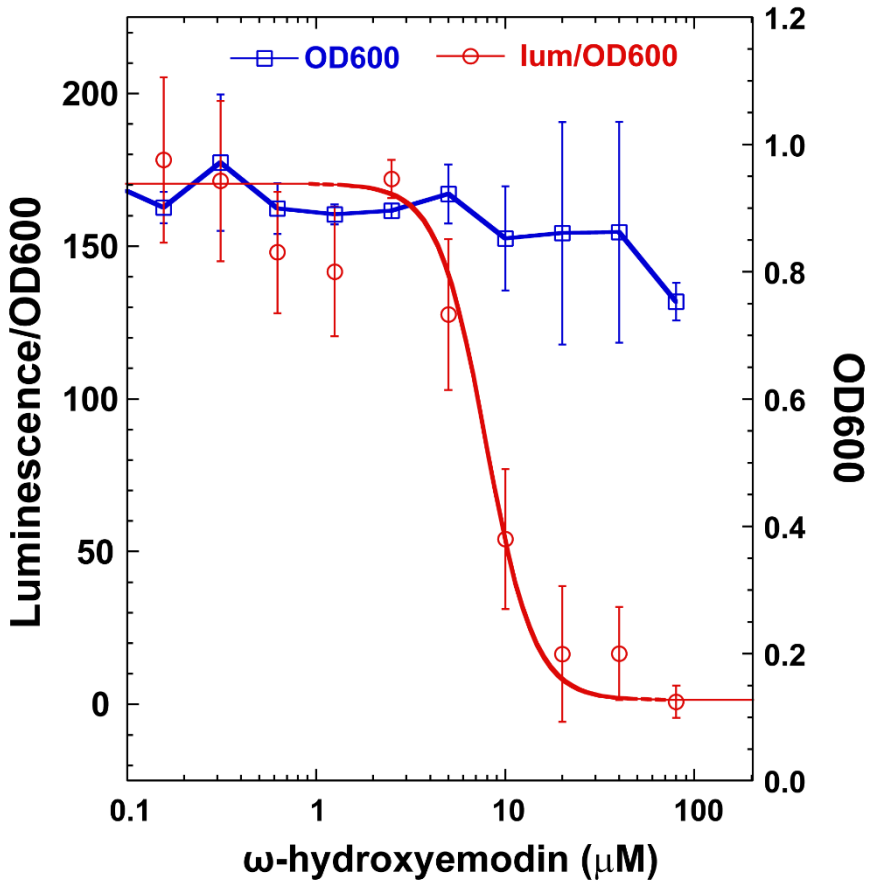

Figure S8. A dose response curve of ω-hydroxyemodin (**3**) against quorum sensing reporter strain AH2759. Growth was assessed by absorbance readings at 600 nm after 15 h incubation (OD_{600}, blue), and bioluminescence was taken at that time point and plotted relative to growth (red). These data indicated that **3** did not significantly inhibit *S. aureus* growth in the concentration range tested as a quorum sensing inhibitor.

Transverse Sectioning of *P. restrictum* Culture Colony and Sample Preparation for DESI-MS Analysis. A single, mature *P. restrictum* colony was excised from a culture plate and cryosectioned to afford 15 μm sections representing the transverse plane; the cryosectioned colony was thaw mounted onto glass microscope slides. The full depth of the culture (~3 mm), consisting of PDA medium with filamentous fungal growth along the ventral surface, was represented in each transverse section. Imaging of the transverse sections was performed under ambient conditions (pressure, temperature, humidity) using DESI-MS. Imaging was performed at a spatial resolution of 200 μm using a solvent system consisting of DMF–CH_3CN (1:1). *Post hoc* processing of the hyperdimensional data provided 2D ion images, retaining spatial relationships and displaying relative mass spectral abundances of particular ions. These plots represent the spatial distributions of these compounds to be investigated with strong molecular discrimination.

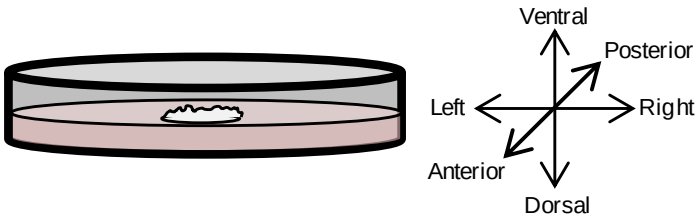

Figure S9. Terms of location used in describing the *P. restrictum* DESI-MS imaging experiments. Transverse plane is defined here as being perpendicular to the anterior-posterior axis.

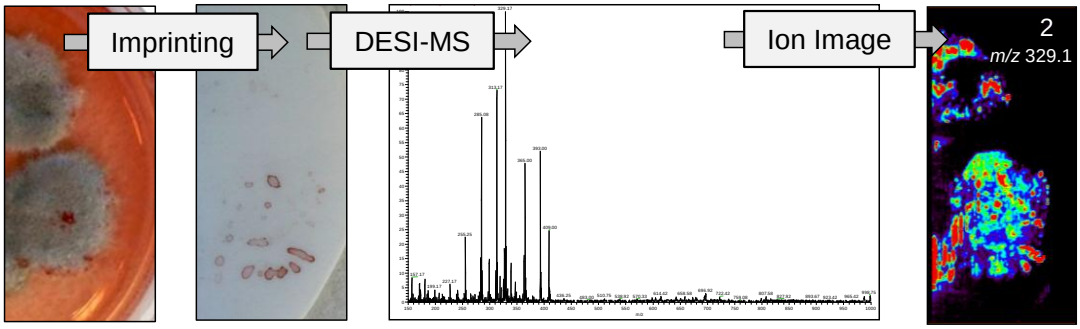

Figure S10. Schematic of imprinting experiment (from left to right): optical image of *P. restrictum* culture, PTFE imprint (pre-mass spectral analysis), representative DESI mass spectrum, and a plotted ion image corresponding to compound **2**, *m/z* 329.1.

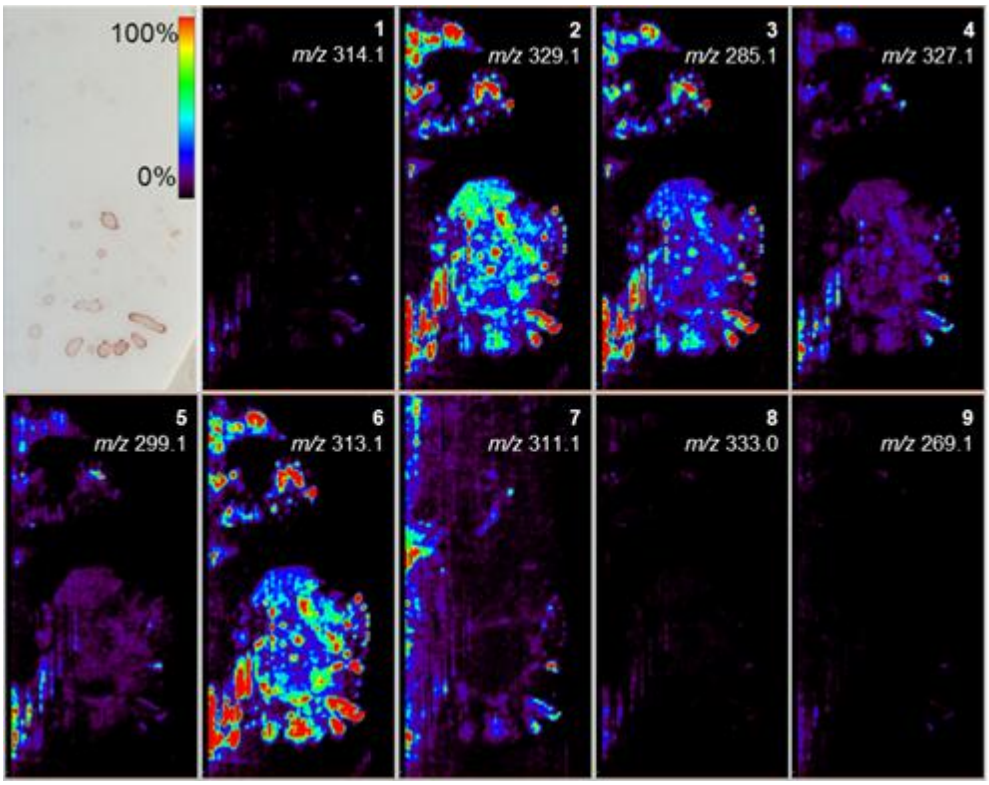

Figure S11. Ion images corresponding to the pseudomolecular ([M–H]$^-$) ions of polyhydroxyanthraquinones **1–9** and optical image of PTFE imprint prior to imaging (upper left). Relative intensities ranging from blue (least abundant) to red (most abundant). The spatial distribution of **1–9** in the ion images and the imprint optical image regions were similar within the limits of the imprinting process. The topography of the culture caused certain regions of the fungal colonies to imprint poorly; for example, the middle region of the upper colony. Note, lines and imaging artifacts are present along the left side of the ion image due to variation in the surface-to-inlet distance. The image corresponding to compound **7** was complicated by an isobaric species that was present in the background.

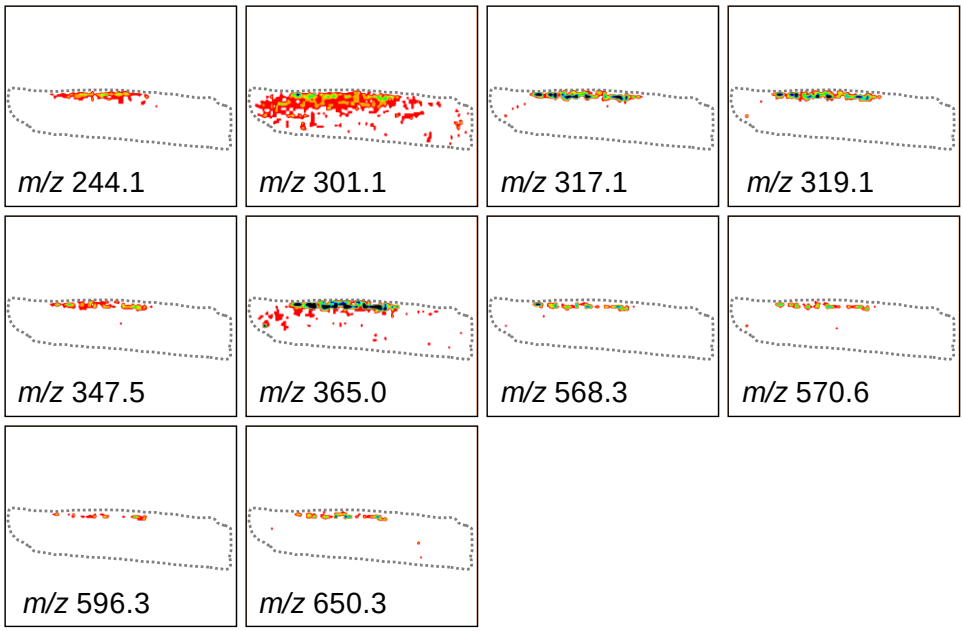

Figure S12. DESI-MS ion images displaying additional ions whose spatial distribution correlate with *P. restrictum*. These ions are presumed to be of fungal origin, given that they were not observed in the analysis of guttate extracts and appear to correlate with fungal presence in the ion images.

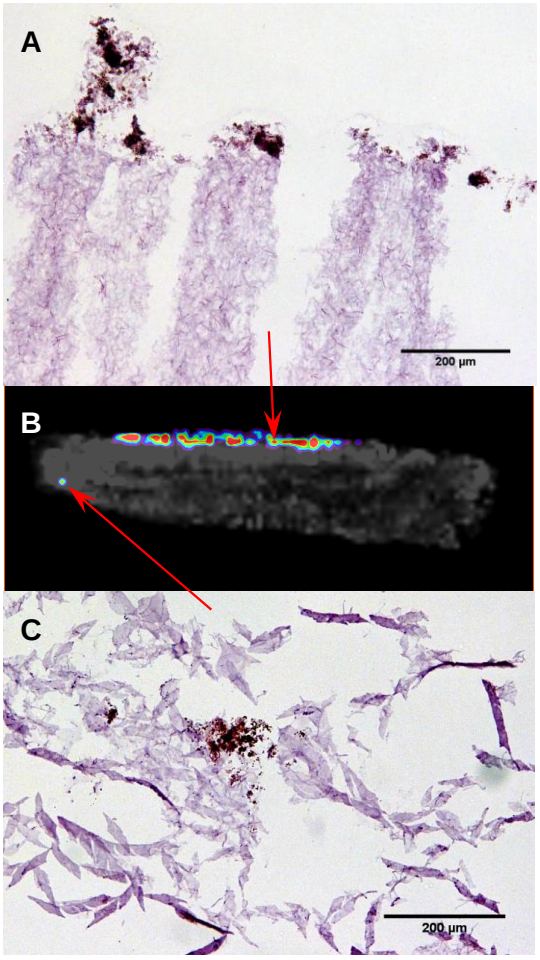

Figure S13. (A) Optical image of a *P. restrictum* section post MS imaging, stained with hematoxylin and eosin. Fungal morphology, stained purple-blue, was detected and location of polyhydroxyanthraquinones was verified by unique alteration in dye color due to reduction-oxidation reactions, stained purple-red. (B) Overlay of two ions present in the mass spectrum, compound **3** (*m/z* 285.1) and **2** (*m/z* 329.1); the coloration of compound **3** ion image reflects relative abundance, whereas *m/z* 329.1 is displayed in grayscale to provide contrast. (C) Zoomed optical image of the region, indicated by red arrow, corresponding to polyhydroxyanthraquinone signal in B.

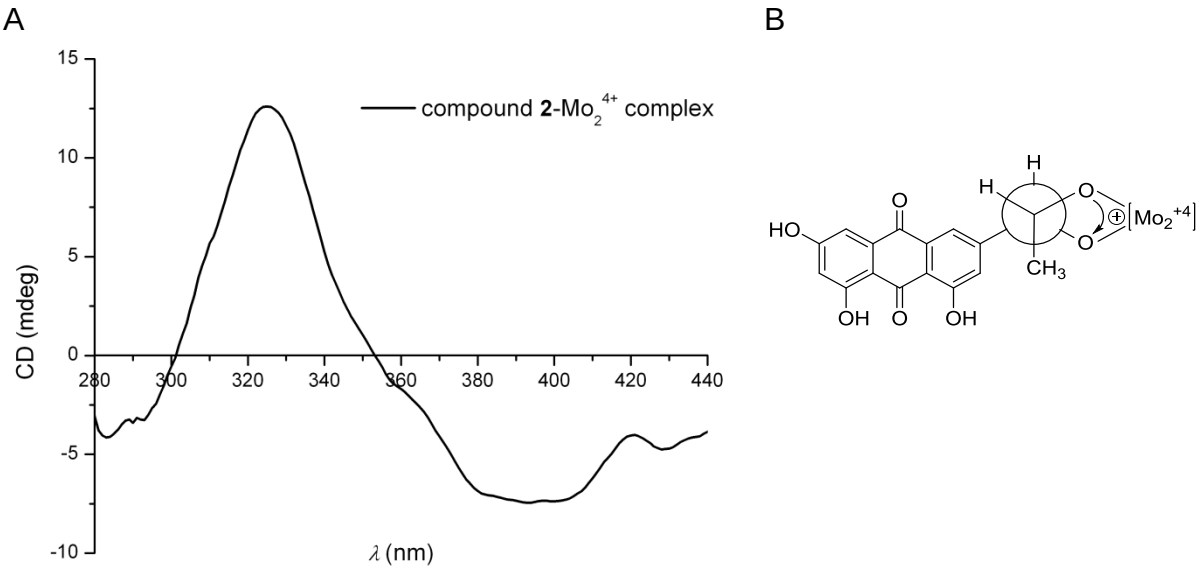

Figure S14. (A) ECD spectrum of compound **2** in a DMSO solution of $Mo_2(OAc)_4$ with inherent ECD spectra subtracted. (B) Conformation of the Mo_2^{4+} complex of **2**.

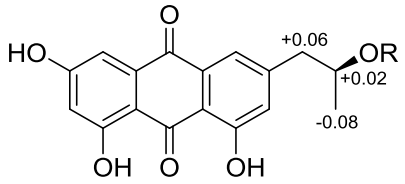

6a: R = (*S*)-MTPA
6b: R = (*R*)-MTPA

Figure S15. $\Delta\delta_H$ values [$\Delta\delta$ (in ppm) = $\delta_S - \delta_R$] obtained for (*S*)- and (*R*)-MTPA esters (**6a** and **6b**, respectively) of (+)-2'*S*-isorhodoptilometrin (**6**) in pyridine-d_5.

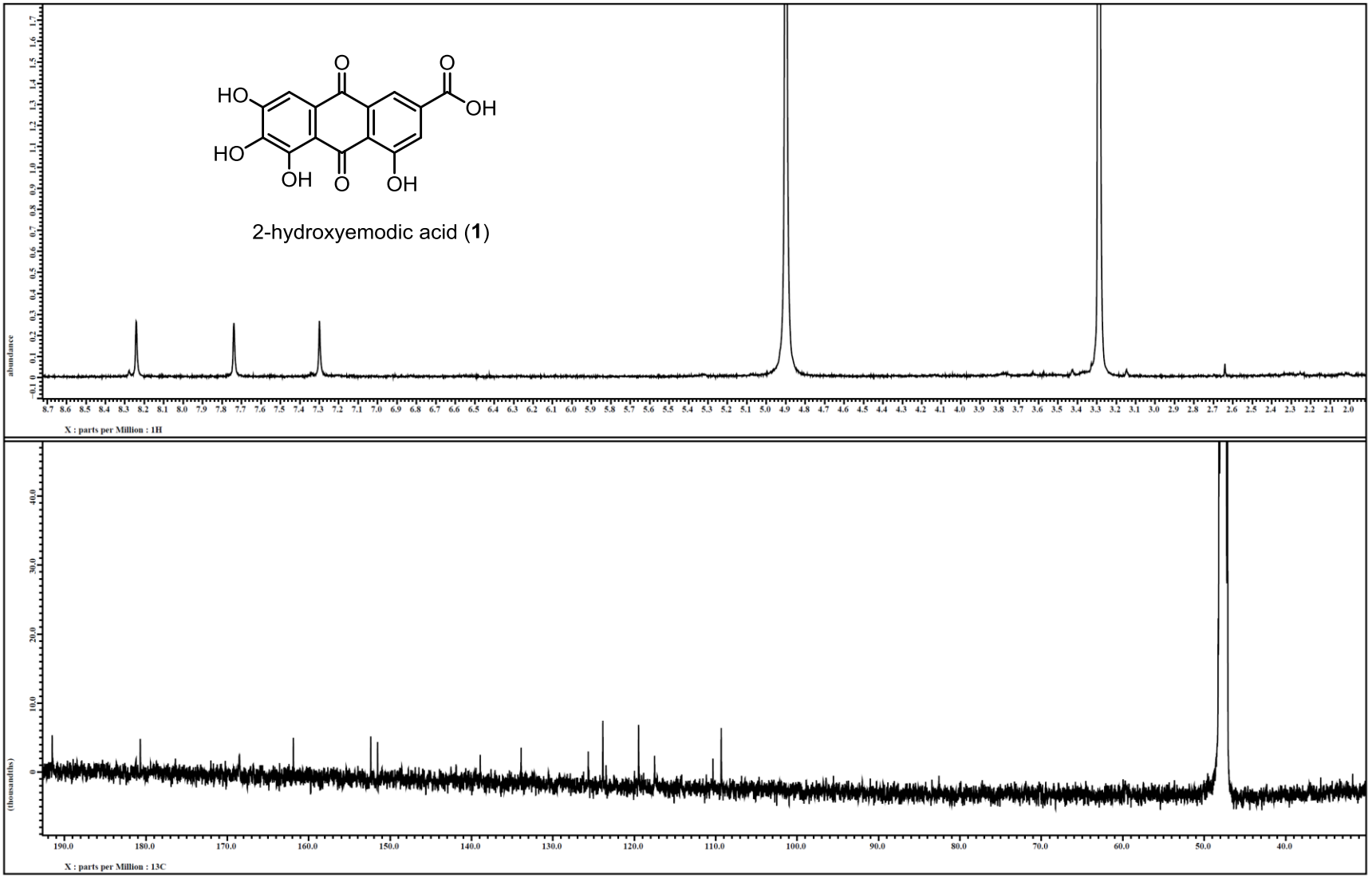

Figure S16. ^{1}H and ^{13}C NMR spectra of compound **1** [500 MHz for ^{1}H and 125 MHz for ^{13}C, methanol-d_4].

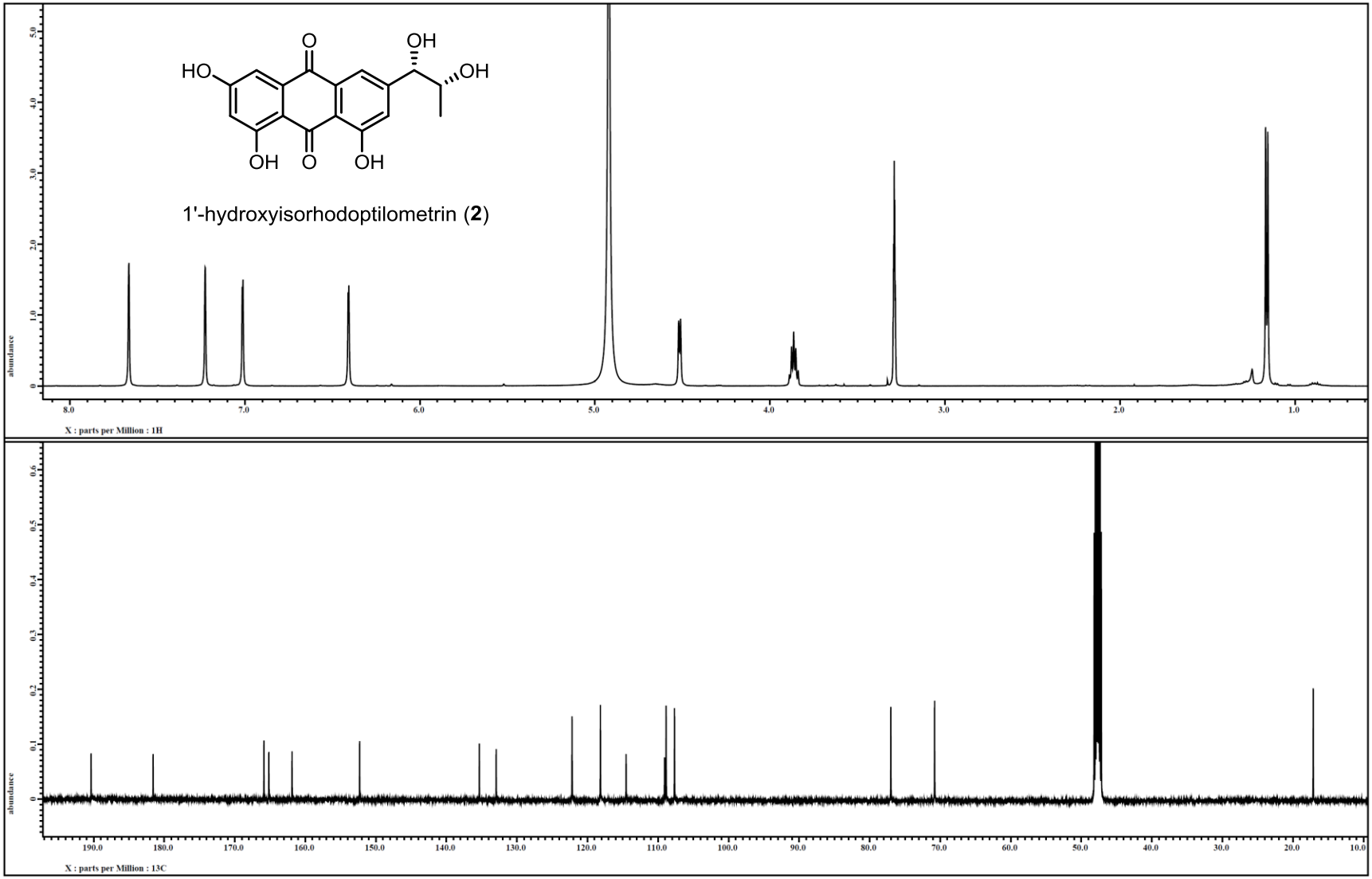

Figure S17. ^{1}H and ^{13}C NMR spectra of compound **2** [500 MHz for ^{1}H and 125 MHz for ^{13}C, methanol-d_4].

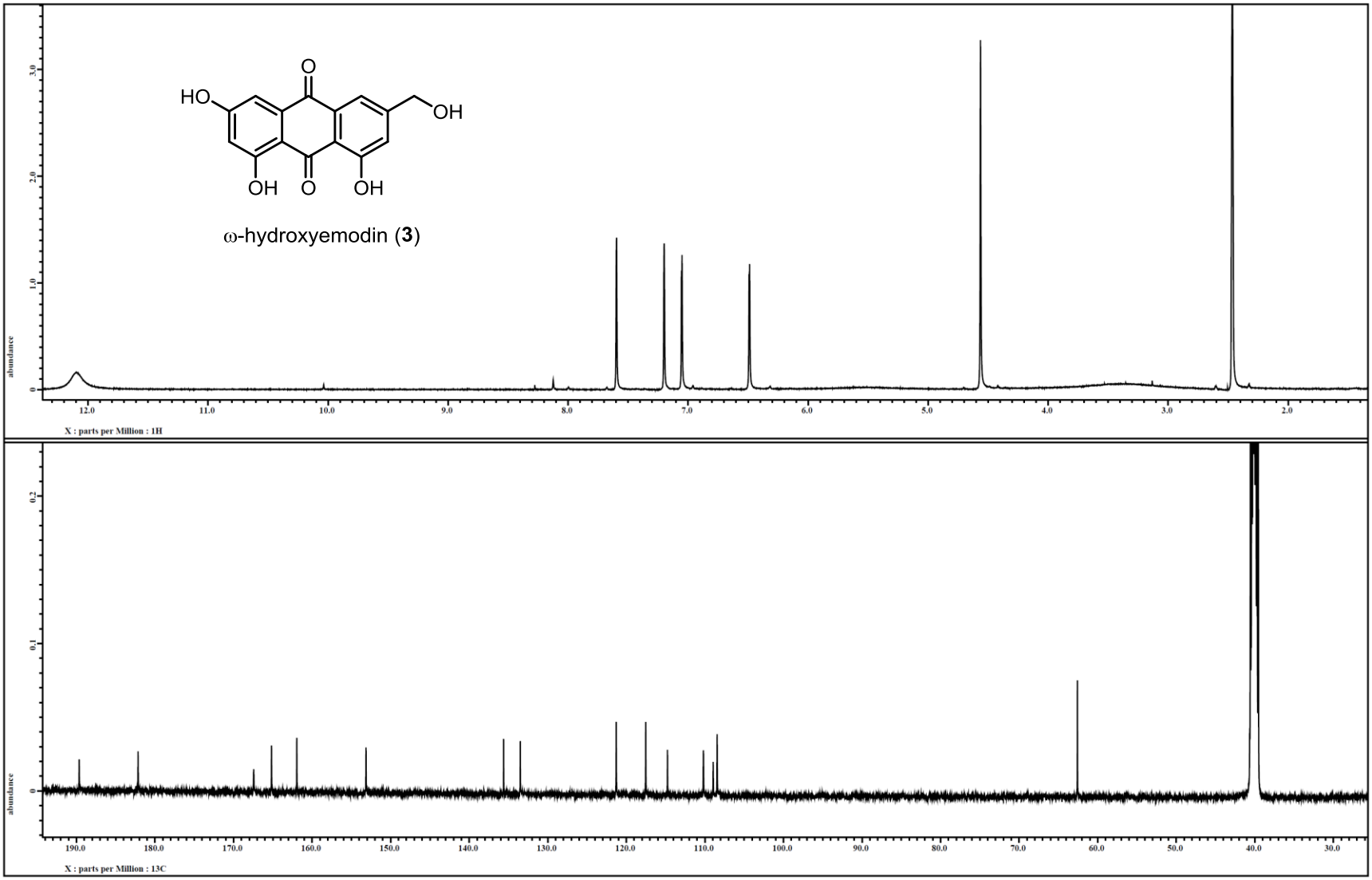

Figure S18. ^{1}H and ^{13}C NMR spectra of compound **3** [500 MHz for ^{1}H and 125 MHz for ^{13}C, DMSO-d_6].

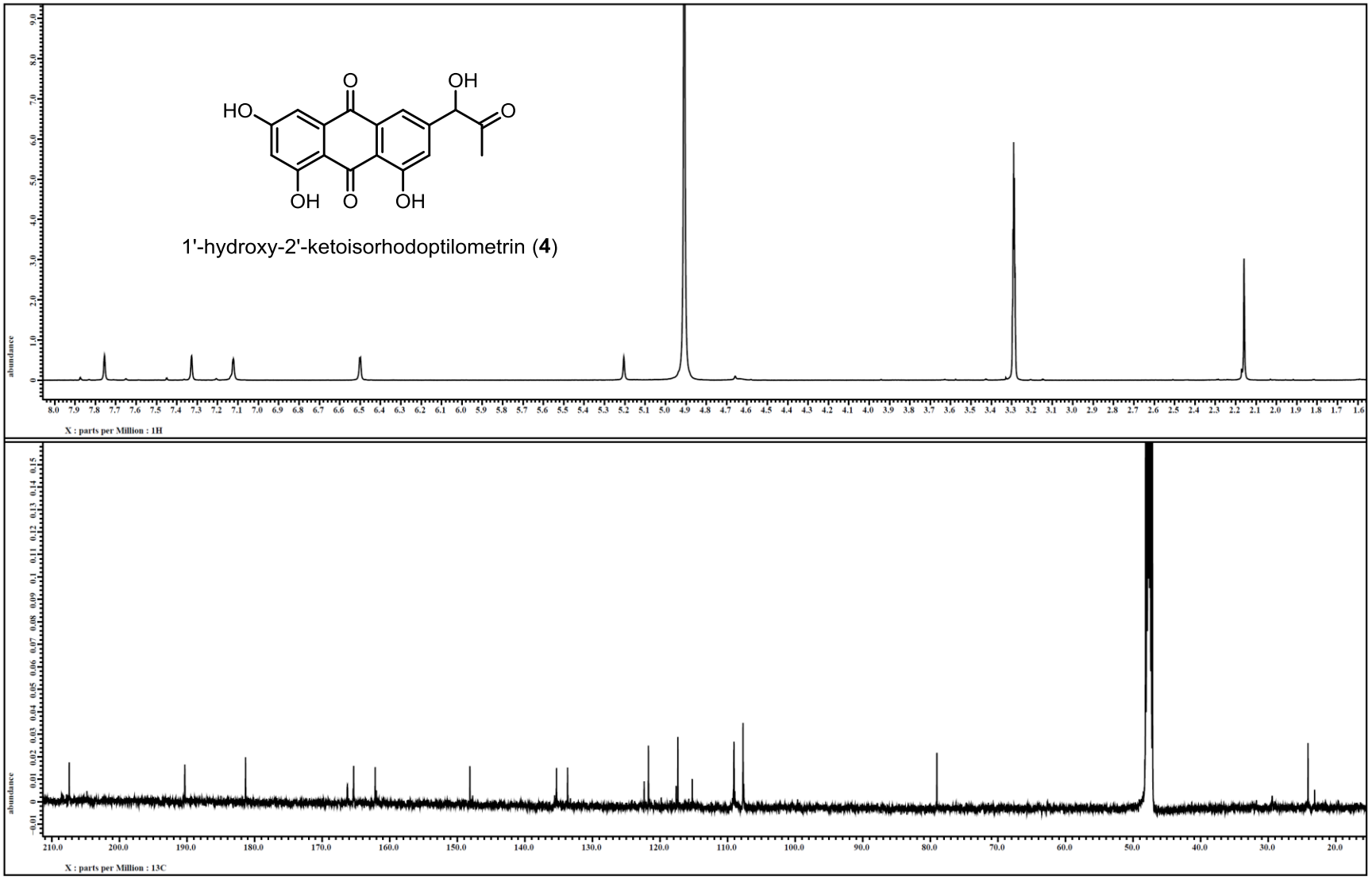

Figure S19. ^{1}H and ^{13}C NMR spectra of compound **4** [500 MHz for ^{1}H and 125 MHz for ^{13}C, methanol-d_4].

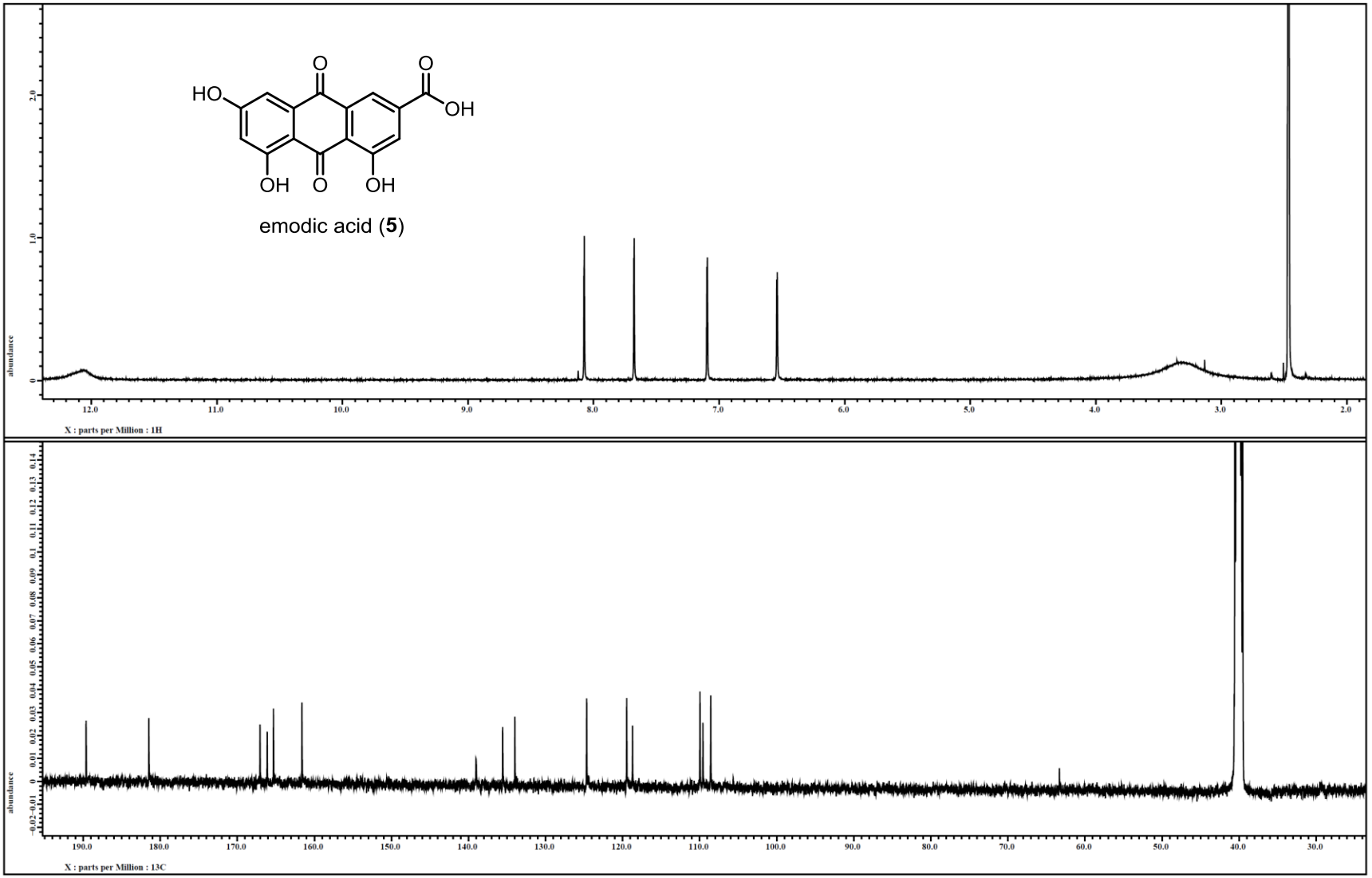

Figure S20. ^{1}H and ^{13}C NMR spectra of compound **5** [500 MHz for ^{1}H and 125 MHz for ^{13}C, DMSO-d_6].

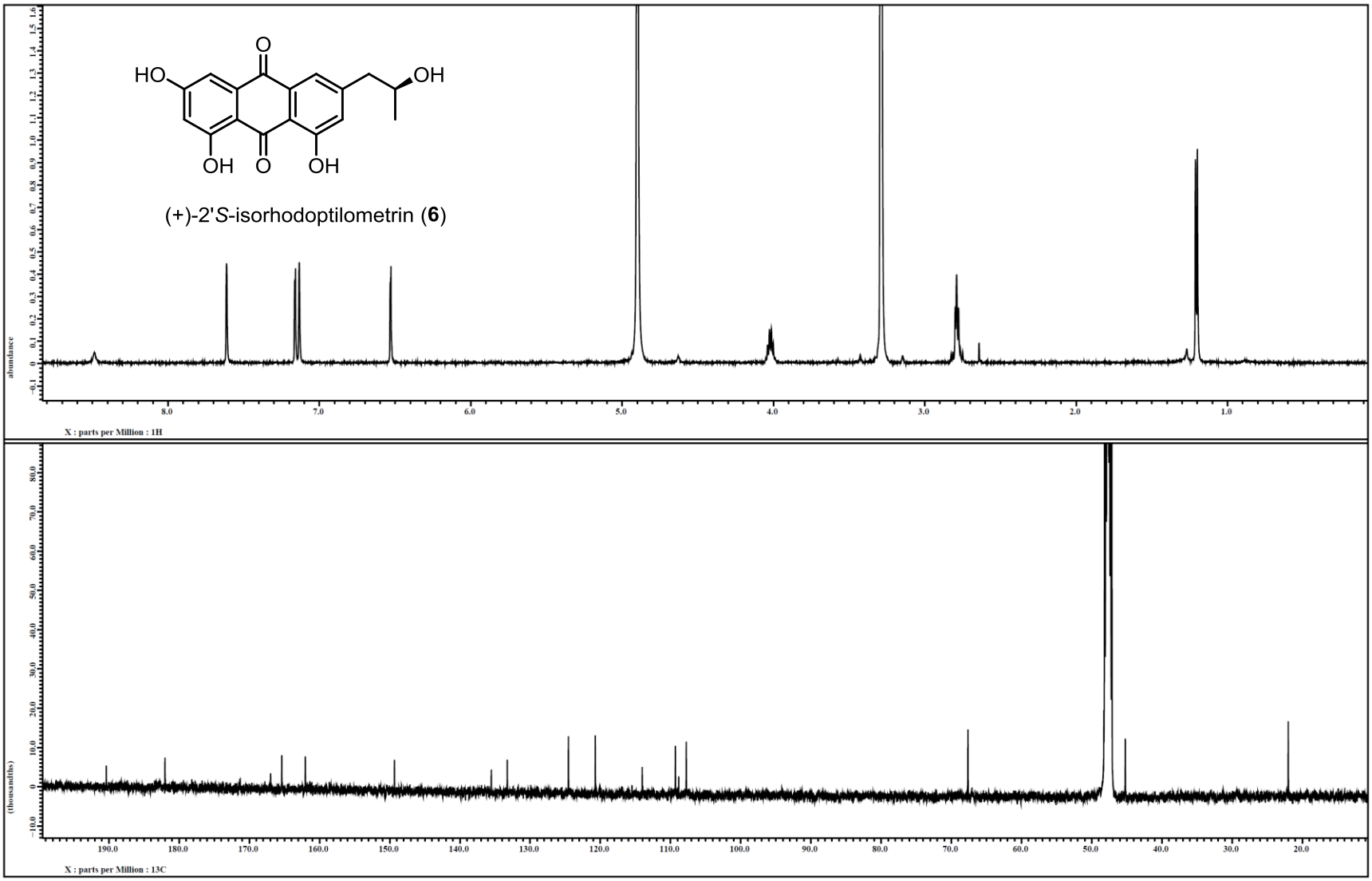

Figure S21. ^{1}H and ^{13}C NMR spectra of compound **6** [500 MHz for ^{1}H and 125 MHz for ^{13}C, methanol-d_4].

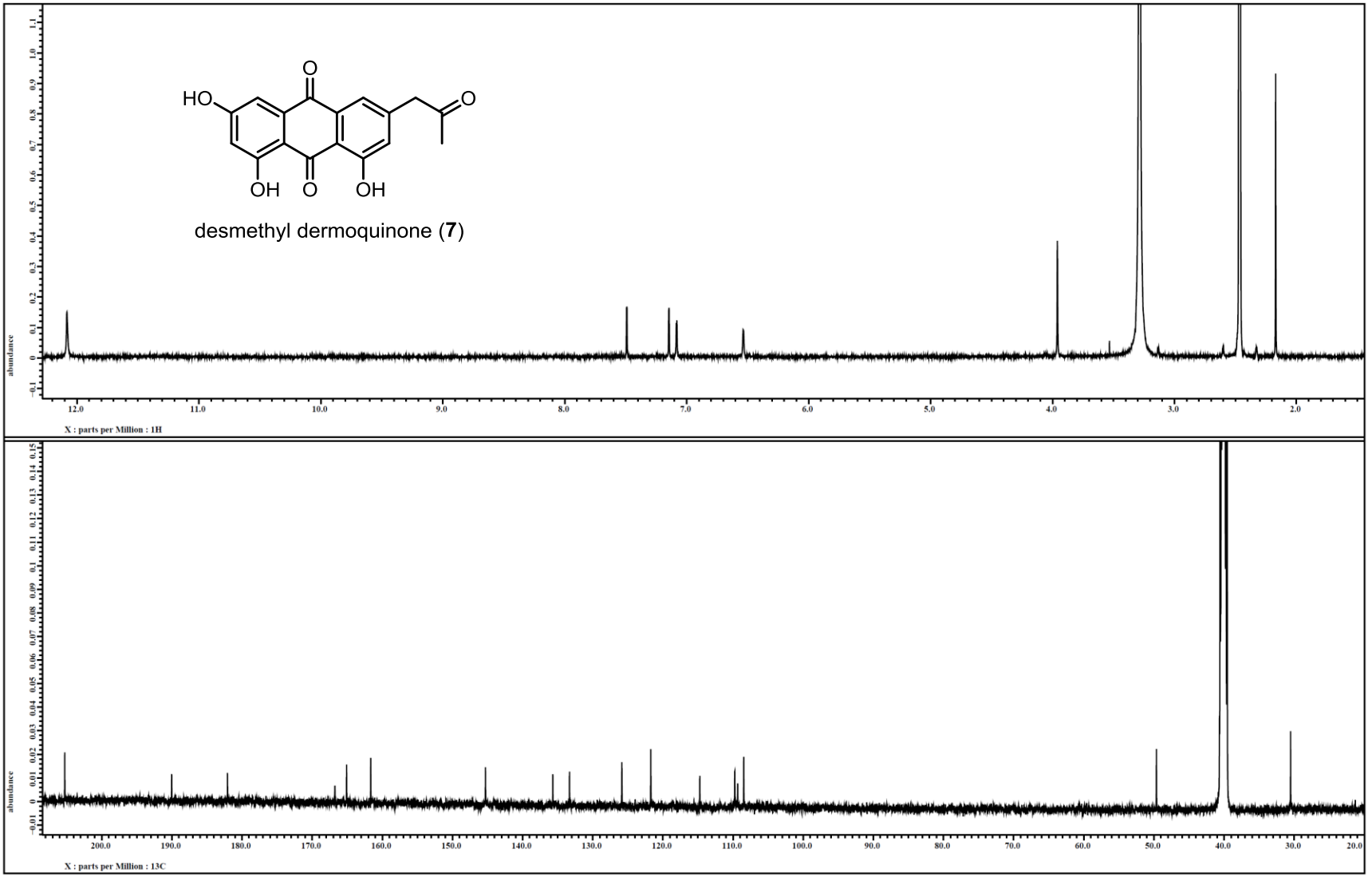

Figure S22. ^{1}H and ^{13}C NMR spectra of compound **7** [500 MHz for ^{1}H and 125 MHz for ^{13}C, DMSO-d_6].

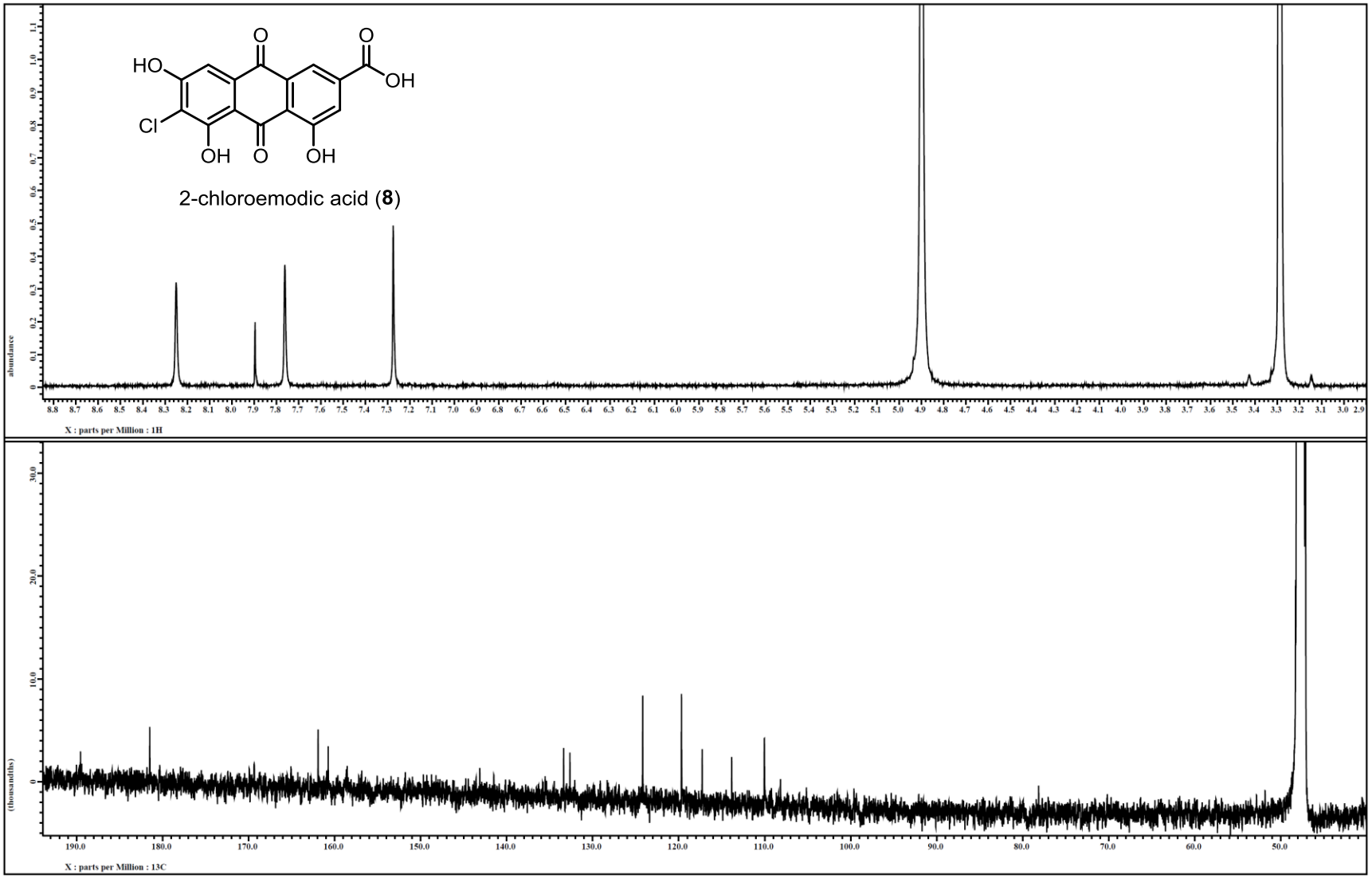

Figure S23. ^{1}H and ^{13}C NMR spectra of compound **8** [500 MHz for ^{1}H and 125 MHz for ^{13}C, methanol-d_4].

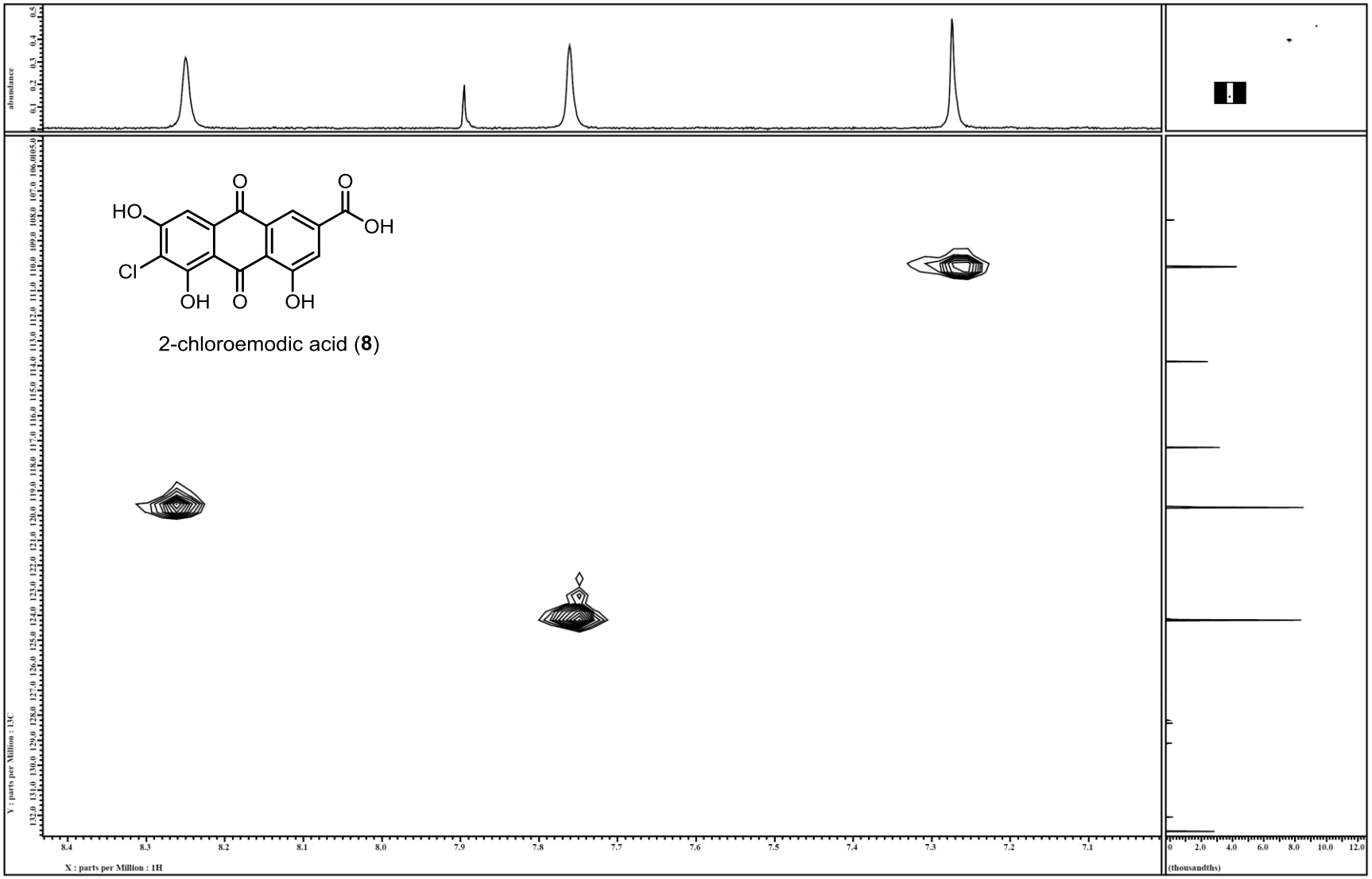

Figure S24. $^{1}H \rightarrow {}^{13}C$ edited-HSQC NMR spectrum of compound **8** [500 MHz, methanol-d_4].

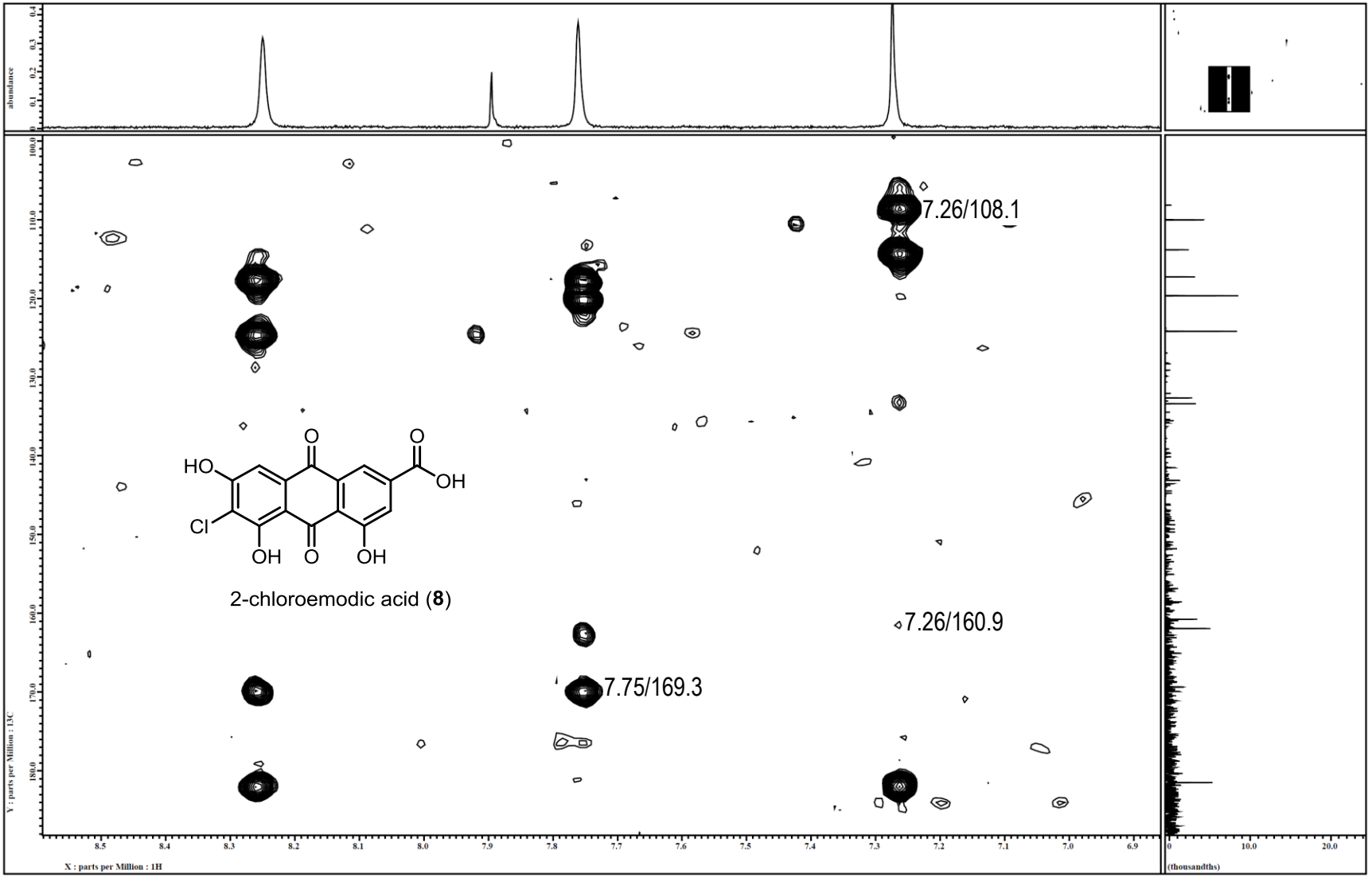

Figure S25. $^{1}H \rightarrow {}^{13}C$ HMBC NMR spectrum of compound **8** [500 MHz, methanol-d_4].

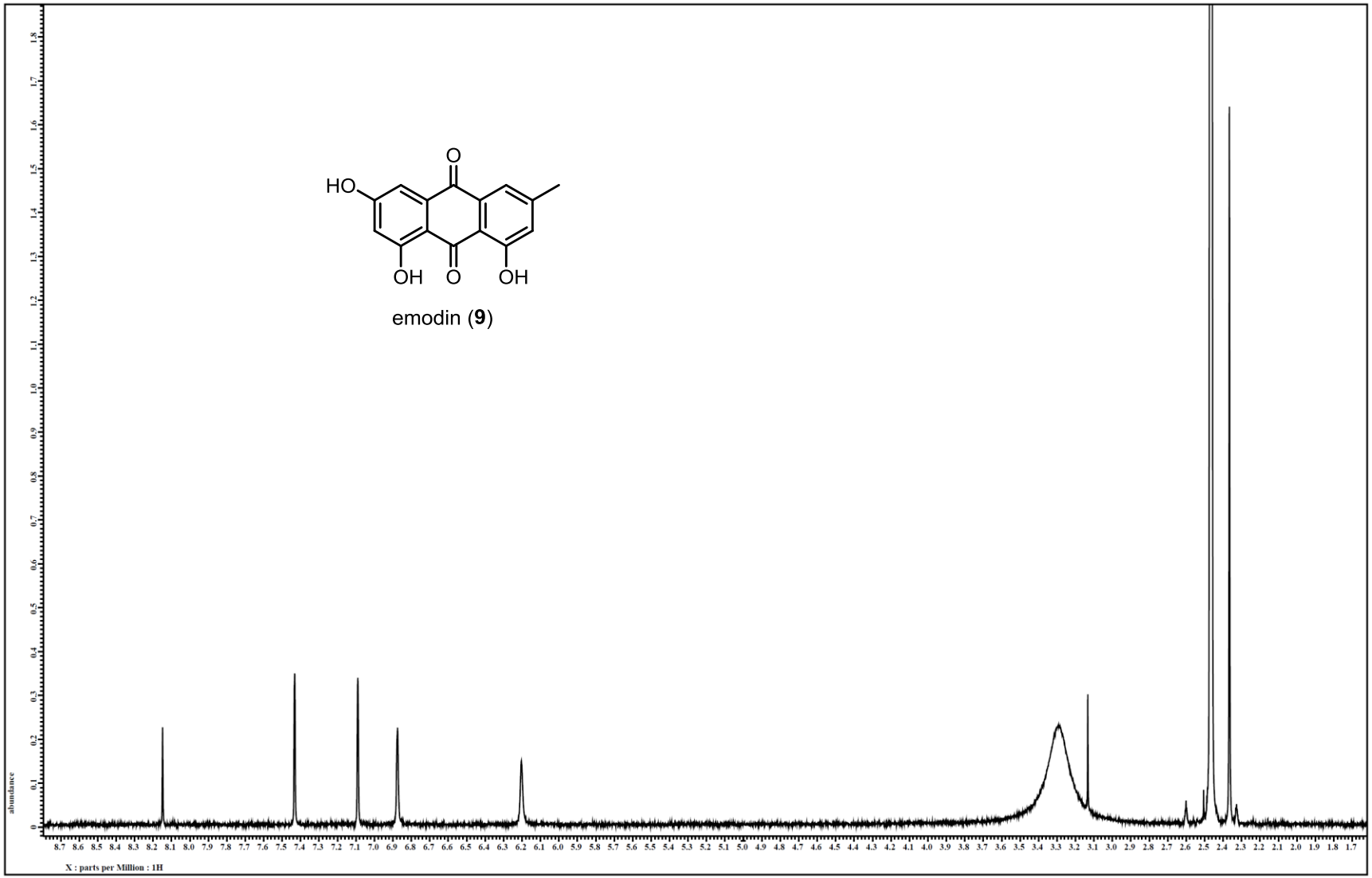

Figure S26. ^{1}H NMR spectrum of compound **9** [500 MHz, DMSO-d_6].

REFERENCES

(1) Houbraken, J.; Samson, R. A. *Stud. Mycol.* **2011,** *70*, 1-51.

(2) El-Elimat, T.; Figueroa, M.; Raja, H. A.; Graf, T. N.; Adcock, A. F.; Kroll, D. J.; Day, C. S.; Wani, M. C.; Pearce, C. J.; Oberlies, N. H. *J. Nat. Prod.* **2013,** *76*, 382-387.

(3) Gardes, M.; Bruns, T. D. *Mol. Ecol.* **1993,** *2*, 113-118.

(4) White, T. J.; Bruns, T. D.; Lee, S. B.; Taylor, J. W. In *PCR Protocols: A Guide to Methods and Application*; Innis, M. A.; Gefland, D. H.; Sninsky, J. J.; White, T. J., Eds.; Academic Press: San Diego, CA, 1990; pp 315-322.

(5) Rehner, S. A.; Samuels, G. J. *Can. J. Bot.* **1995,** *73*, S816-S823.

(6) Vilgalys, R.; Hester, M. *J. Bacteriol.* **1990,** *172*, 4238-4246.

(7) Schmitt, I.; Barker, F. K. *Nat. Prod. Rep.* **2009,** *26*, 1585-1602.

(8) Peterson, S. W. In *Integration of Modern Taxonomic Methods for Penicillium and Aspergillus Classification* Samson, R. A.; Pitt, J. I., Eds.; Plenum Press: New York, NY, 2000; pp 163-178.

(9) Peterson, S. W. *Appl. Microbiol. Biotechnol.* **2012,** *95*, 339-344.

(10) Miller, A. N.; Huhndorf, S. M. *Mol. Phylogenet. Evol.* **2005,** *35*, 60-75.

(11) Tamura, K.; Peterson, D.; Peterson, N.; Stecher, G.; Nei, M.; Kumar, S. *Mol. Biol. Evol.* **2011,** *28*, 2731-2739.

(12) Hillis, D. M.; Bull, J. J. *Syst. Biol.* **1993,** *42*, 182-192.

(13) Raja, H. A.; Oberlies, N. H.; El-Elimat, T.; Miller, A. N.; Zelski, S. E.; Shearer, C. A. *Mycoscience* **2013,** *54*, 353-361.

(14) Di Bari, L.; Pescitelli, G.; Pratelli, C.; Pini, D.; Salvadori, P. *J. Org. Chem.* **2001,** *66*, 4819-4825.

(15) Frelek, J.; Snatzke, G.; Szczepek, W. J. *Fresenius J. Anal. Chem.* **1993,** *345*, 683-687.

(16) Snatzke, G.; Wagner, U.; Wolff, H. P. *Tetrahedron* **1981,** *37*, 349-361.

(17) Chen, H.; Cotte-Rodriguez, I.; Cooks, R. G. *Chem. Commun.* **2006**, 597-599.

(18) Hall, D. G. In *Boronic Acids: Preparation and Applications in Organic Synthesis and Medicine*; Hall, D. G., Ed.; Wiley-VCH Verlag GmbH & Co.: Weinheim, F.R.G., 2006; pp 1-100.

(19) Hoye, T. R.; Jeffrey, C. S.; Shao, F. *Nat. Protoc.* **2007,** *2*, 2451-2458.

(20) Powell, V. H.; Sutherland, M. D. *Aust. J. Chem.* **1967,** *20*, 541-553.

(21) Khamthong, N.; Rukachaisirikul, V.; Tadpetch, K.; Kaewpet, M.; Phongpaichit, S.; Preedanon, S.; Sakayaroj, J. *Arch. Pharm. Res.* **2012,** *35*, 461-468.

(22) Ren, H.; Tian, L.; Gu, Q.; Zhu, W. *Arch. Pharm. Res.* **2006,** *29*, 59-63.

(23) Arioka, S.; Sakagami, M.; Uematsu, R.; Yamaguchi, H.; Togame, H.; Takemoto, H.; Hinou, H.; Nishimura, S. *Bioorg. Med. Chem.* **2010,** *18*, 1633-1640.

(24) Kemami Wangun, H. V.; Wood, A.; Fiorilla, C.; Reed, J. K.; McCarthy, P. J.; Wright, A. E. *J. Nat. Prod.* **2010,** *73*, 712-715.

(25) Frelek, J.; Geiger, M.; Voelter, W. *Curr. Org. Chem.* **1999,** *3*, 117-146.

(26) Frelek, J.; Ikekawa, N.; Takatsuto, S.; Snatzke, G. *Chirality* **1997,** *9*, 578-582.